Earth Syst. Sci. Data Discuss., 7, 1–57, 2014
www.earth-syst-sci-data-discuss.net/7/1/2014/
doi:10.5194/essdd-7-1-2014

Open Access Earth System Science Data Discussions

Temperature data acquired from the DOI/GTN-P Deep Borehole Array on the Arctic Slope of Alaska, 1973–2013

G. D. Clow

US Geological Survey, Boulder, Colorado, USA

Received: 3 December 2013 – Accepted: 24 December 2013 – Published: 20 January 2014

Correspondence to: G. D. Clow (clow@usgs.gov)

Published by Copernicus Publications.

Abstract

A homogeneous set of temperature measurements obtained from the DOI/GTN-P Deep Borehole Array between 1973 and 2013 is presented. The 23-element array is located on the Arctic Slope of Alaska, a region of cold continuous permafrost. Most of the monitoring wells are situated on the arctic coastal plain between the Brooks Range and the Arctic Ocean, while others are in the foothills to the south. The data represent the true temperatures in the wellbores and surrounding rocks at the time of the measurements; they have not been corrected to remove the thermal disturbance caused by drilling the wells. With a few exceptions, the drilling disturbance is estimated to have been of order 0.1 K or less by 1989. Thus, most of the temperature measurements acquired during the last 25 yr are little affected by the drilling disturbance. The data contribute to ongoing efforts to monitor changes in the thermal state of permafrost in both hemispheres by the Global Terrestrial Network for Permafrost (GTN-P), one of the primary subnetworks of the Global Terrestrial Observing System (GTOS). The data will also be useful for refining our basic understanding of the physical conditions in permafrost in arctic Alaska, as well as provide important information for validating predictive models used for climate impact assessments. The processed data are available from the ACADIS repository at doi:10.5065/D6N014HK.

1 Introduction

The Arctic is highly sensitive to increases in global mean temperature as exemplified by the large and persistent physical and biological changes currently being observed there (Jeffries et al., 2012, 2013). In turn, the Arctic can have a significant impact on the global climate system through ice-albedo feedbacks and the potential loss of vast amounts of methane (a potent greenhouse gas) stored in permafrost to the atmosphere. Despite this, the Arctic remains a data-spare region, limiting our understanding of critical processes and our ability to project future environmental conditions. To ad-

ESSDD
7, 1–57, 2014

Temperature data from the DOI/GTN-P Deep Borehole Array

G. D. Clow

dress this issue, several initiatives have been undertaken to develop comprehensive observing systems for the atmosphere, ocean, and terrestrial components of the arctic climate system (e.g, the Sustaining Arctic Observing Networks initiative). These observing systems are generally built from an aggregation of many national or regional observing networks. The success of these comprehensive observing systems critically depends on the contributions from the individual networks.

Here we focus on one such network designed to monitor the thermal state of permafrost on the Arctic Slope of Alaska. The origin of the network began 40 yr ago. From 1975 to 1981, 28 test wells were drilled in the National Petroleum Reserve–Alaska (NPR-A) as part of a petroleum exploration program overseen by the US Department of the Interior (Gryc, 1988). These 1–6 km deep wells penetrated marine and non-marine sedimentary sequences between the Brooks Range and the Arctic Ocean. Most of the well sites are on the low-lying arctic coastal plain while a few are in the rolling foothills to the south. Permafrost in this area is "continuous", being 200–400 m thick. As with all deep wells, temperatures in the wellbores and surrounding rocks were significantly disturbed by the addition of drilling muds, circulating fluids, and other processes during drilling. This thermal drilling disturbance eventually dissipates over many years (Lachenbruch and Brewer, 1959). Wells drilled by the petroleum industry on the Arctic Slope of Alaska were almost always either put into production or plugged and abandoned long before the wells could return to thermal equilibrium. Realizing the NPR-A test wells provided a rare opportunity to obtain "undisturbed" temperatures in permafrost, the US Geological Survey (USGS) requested that 21 of the wells (Fig. 1, Table 1) be completed in a manner that would allow high-precision temperature measurements to be made over many years. This involved filling the borehole casing with a non-freezing fluid (diesel oil) above a cement plug installed 200–900 m below the surface, depending on the well. Four other wells to the east were preserved in a similar manner through the courtesy of Mobil, Exxon, BP, Sinclair, and Forest Oil Companies. Information obtained from the borehole temperature measurements was expected to provide better estimates for the depth of permafrost and of the physical conditions con-

ESSDD
7, 1–57, 2014

trolling the occurrence of ice, unfrozen water, and gas hydrates in permafrost than was currently available.

After monitoring temperatures in these wells for several years, it became clear that the temperature profiles also contained evidence of recent climate change in arctic Alaska. The theory behind this climate-change effect is that any change in the surface energy balance would generate a downward propagating thermal wave. Without the disruptive effects of groundwater flow, this thermal wave is effectively preserved in cold continuous permafrost, although the magnitude of the signal dissipates over time. With sufficiently sensitive instruments, a climate-induced thermal wave could be detected and the associated change in surface temperature inferred. Using this idea and temperatures from the NPR-A monitoring wells and from the nearby Prudhoe Bay oil field, Lachenbruch published a series of papers in the 1980s (Lachenbruch et al., 1982, 1988b; Lachenbruch and Marshall, 1986) in which he inferred surface temperatures in the Alaskan Arctic had warmed 2–4 K during the previous few decades. Given the paucity of long-term instrumental records in the Arctic documenting recent climate change, Lachenbruch's work was particularly important. Soon thereafter, other researchers began to use subsurface permafrost temperatures to document recent climate changes in the North American Arctic, for example: Nielsen and Beck (1989); Mareschal and Beltrami (1992); Beltrami and Mareschal (1992); Osterkamp and Romanovsky (1999); Smith et al. (2005); Osterkamp and Jorgenson (2006); Taylor et al. (2006).

In 1999, the 21 NPR-A temperature-monitoring wells were incorporated into the Global Terrestrial Network for Permafrost (GTN-P), a new component of the Global Climate Observing System (GCOS) and one of its primary subnetworks, the Global Terrestrial Observing System (GTOS). This formalized the use of the borehole array for monitoring the *thermal state of permafrost* (TSP), one of the Essential Climate Variables (ECVs) tracked by the global climate observing systems (Sessa and Dolman, 2008; Smith and Brown, 2009). Upon inclusion into GTN-P, the NPR-A wells became one of the largest arrays of deep (> 125 m) boreholes in the world used for monitor-

ESSDD
7, 1–57, 2014

ing temperatures in permafrost (IPA, 2010). As management of the array was shared by two US Department of the Interior (DOI) agencies (USGS and the Bureau of Land Management), the array became known as the DOI/GTN-P Deep Borehole Array. Two of the four wells that had been preserved for USGS temperature monitoring to the east of the NPR-A (Lupine and Echooka, Fig. 1, Table 1) were later incorporated into GTN-P, bringing the total number of wells in the DOI/GTN-P Borehole Array to 23. Beginning in 1998, USGS also began deploying automated climate-monitoring stations in the NPR-A to better understand the nature of the recent permafrost warming observed there. Nine of the climate stations were co-located with DOI/GTN-P boreholes to form "permafrost observatories" (Table 1), although two of the boreholes were subsequently plugged and abandoned due to the threat of coastal erosion. Data from the DOI/GTN-P climate stations are available from Urban and Clow (2014).

Here we present the temperature data acquired from the DOI/GTN-P Borehole Array in arctic Alaska over the 40 yr period, 1973–2013. The data represent the true temperatures in the wellbores and surrounding rocks at the time of the measurements; they have not been "corrected" to remove the thermal disturbance caused by drilling the wells. For the great majority of wells, the drilling disturbance is estimated to have been of order 0.1 K or less by 1989. Thus, most of the temperature measurements acquired over the last 25 yr are little affected by the drilling disturbance. The dataset presented here is intended to serve as the reference point from which datasets corrected for the drilling disturbance will be derived, enhancing the usefulness of the earlier temperature logs. In addition, analysis of the uncorrected temperature logs can provide important information about the ice and unfrozen water content in the permafrost zone. As shown in Fig. 2, temperature measurements in the DOI/GTN-P monitoring wells were concentrated during distinct field campaigns that occurred during 1977–1984, 1989, 2002–2003, 2007–2008, and 2012–2013. Measurements were curtailed during the 1990s due to funding limitations, except for a few experimental logs designed to test design changes in the temperature logging system. Measurements were resumed in 2002 under a GTN-P protocol specifying that contributing deep borehole arrays be

ESSDD
7, 1–57, 2014

resampled every 5 yr (Fig. 3). By 2010, four of the monitoring wells (ATI, DRP, ETK, JWD) had been plugged and abandoned due to coastal erosion and were no longer accessible. Data from the DOI/GTN-P Borehole Array will be useful for documenting how the thermal state of permafrost is changing on the Arctic Slope of Alaska in response to climate change. Given the important role that permafrost has in shaping the regional landscape, this information is critical for understanding how lakeshore, river, and coastal environments may change in the near future; anticipating impacts on terrestrial ecosystem habitats; and for making well-informed land management decisions in the face of rapid climate change. The data will also be useful for refining our basic understanding of the physical conditions occurring within permafrost in this region.

2 Instruments and methods

2.1 Borehole temperature measurements

The "portable" logging system used by the US Geological Survey to measure temperatures in the DOI/GTN-P boreholes consists of a custom temperature sensor whose resistance is determined by a resistance readout (digital multimeter) using a 4-wire Kelvin circuit. This circuit effectively compensates for the resistance of the logging cable and various connectors that provide the electrical path between the downhole temperature sensor and the resistance readout located on the surface (Fig. 4). The temperature sensor consists of a parallel-series network of negative-temperature-coefficient (NTC) thermistors hermitically sealed in glass. These in turn are enclosed in a thin (4 mm diameter) stainless steel shell to isolate the thermistors from pressure effects and corrosive chemicals. The resulting probe design has proved to be rugged and stable, and provides a high temperature sensitivity (Sass et al., 1971; Clow, 2008).

Several refinements have been made to the portable system since the 1970s when measurements began in the DOI/GTN-P boreholes. To minimize weight, the early version of the system did not have a slip-ring assembly. Temperatures were measured

ESSDD
7, 1–57, 2014

at fixed depths, typically every 1.5 or 3.0 m, and the logging cable disconnected from the resistance readout when moving from one measurement depth to the next. At each depth, measurements were made until the sensor approached thermal equilibrium with the surrounding environment. A high-quality slip-ring connector was introduced to the system in 1984, allowing measurements to be acquired while the sensor was moving continuously downhole; a circuit triggered the system to acquire a measurement every 30 cm. The depth and sensor resistance measurements were automatically recorded on magnetic tape. A logging speed of $\sim 10\,\mathrm{cm\,s^{-1}}$ was used with this system.

One disadvantage of the rugged probe design is the relatively slow response time ($\tau \in 7$–15 s). Given the thermal memory of the probe, a time deconvolution is required to determine the actual temperature at any given depth from the temperature measurements while the sensor is moving. To assist with the deconvolution, the resistance readout was upgraded in 1991 enabling measurements to be triggered on even time increments (every 2 s) while a computer provided the time of each triggering event. The primary data stream then consisted of time, depth, and sensor resistance. The logging speed was also reduced to 2.5–5 $\mathrm{cm\,s^{-1}}$ to reduce the magnitude of the deconvolution correction. With a triggering rate of 2 s, this decreased the depth interval between measurements to 5–10 cm. An additional change aimed at improving the results of the time deconvolution was to replace the hydraulic clutch that regulated the probe descent with a motor drive to reduce variations in the probe's downhole speed. The new resistance readout also offered 10 times the resolution while simultaneously reducing the test current I_s by a factor of ten. The latter feature reduced the heating of the thermistor beads during a measurement due to the test current by 10^2. Utilizing another capability of the new readout, the measuring circuit was recalibrated before each temperature log using a set of "standard" resistors.

Efforts were made through the 1990s to further reduce the uncertainty of the resistance measurements. Issues that were addressed included drift of the measurement circuitry due to environmental changes during a log and spurious electrical noise caused by the winch motor, the presence of the system operator, blowing snow, and

ESSDD
7, 1–57, 2014

other sources. By 1999, these issues were effectively resolved by locating the resistance readout in a Faraday cage maintained at 23 ± 0.5 °C for the duration of a logging experiment. The system has changed little since that time. A complete description of the current system (Fig. 5) and the associated measurement uncertainties is given by Clow (2008). Although a complete uncertainty analysis was not done for the early version of the portable system, Sass et al. (1971) and Lachenbruch et al. (1988a) state that the precision of the measurements was better than 0.01 K while the absolute accuracy was "probably only a few hundredths of a degree". This level of uncertainty persisted through at least 1991. The standard uncertainty of the ITS-90 temperature measurements made with the current (post-1999) logging system ranges from 3.0 mK at −60 °C to 3.3 mK at 0 °C.

2.2 Data processing

The processing of the temperature logs consists of several steps that depends on whether the data were acquired at fixed depth intervals (pre-1984) or while the sensor was moving continuously downhole. For the continuously obtained data, the processing steps include: (1) correcting the measured resistances for systematic biases, (2) converting the resistances to temperature, (3) removing noise from the signal, and (4) deconvolving the signal to correct for the thermal memory of the probe. The last step is unnecessary for the fixed interval data.

2.2.1 Resistance corrections

Several sources of systematic error exist for the temperature-sensor resistance measurements. These include: (a) leakage currents between the conductors of the Kelvin circuit due to dirt, moisture, or imperfections in the conductor insulation, (b) capacitance effects, (c) heating of the probe due to the passage of the test current, and (d) thermal EMFs (thermoelectric voltages). These sources are discussed in detail by Clow (2008).

ESSDD
7, 1–57, 2014

The magnitude of the associated resistance offsets can be summarized as follows:

$$\delta R_\mathrm{l} = \frac{R_\mathrm{s}^2}{R_\mathrm{s} + R_\mathrm{l}} \quad \text{(leakage currents)} \tag{1}$$

$$\delta R_\mathrm{c} = R_\mathrm{s} C \frac{\partial R_\mathrm{s}}{\partial t} \quad \text{(capacitance effects)} \tag{2}$$

$$\delta R_\mathrm{h} = \frac{\alpha_\mathrm{T} (I_\mathrm{s} R_\mathrm{s})^2}{P_\mathrm{d}} \quad \text{(self heating)} \tag{3}$$

$$\delta R_\mathrm{e} = \frac{V_\mathrm{emf}}{I_\mathrm{s}} \quad \text{(thermal EMFs)} \tag{4}$$

where R_s is the probe resistance, R_l is the interconductor resistance, C is the circuit capacitance, I_s is the test current, V_emf is the sum of the thermoelectric voltages, α_T is the sensors's temperature coefficient of resistance ($\alpha_\mathrm{T} \equiv R_\mathrm{s}^{-1}\, \partial R_\mathrm{s} / \partial T$), P_d is the sensor's power dissipation constant, T is temperature, and t is time. In an attempt to correct for the systematic biases, Eqs. (1)–(4) are applied as corrections to the resistance $\tilde{R}_\mathrm{s}$ measured by the logging system's resistance readout to obtain an estimate of the temperature sensor's true resistance,

$$R_\mathrm{s} = \tilde{R}_\mathrm{s} + (\delta R_\mathrm{l} + \delta R_\mathrm{c} + \delta R_\mathrm{h} - \delta R_\mathrm{e}). \tag{5}$$

Expressed in terms of temperature, these corrections are generally limited to 0.1–0.2 mK. No attempt was made to correct the pre-1991 resistance measurements because the magnitude of the corrections is less than the resolution of the pre-1991 resistance readout.

2.2.2 Resistance-to-temperature conversion

Prior to borehole logging experiments, each sensor is calibrated in a temperature calibration bath at the USGS. A standard platinum resistance thermometer (SPRT) certified by the US National Institute of Standards and Technology is used as the calibration

ESSDD
7, 1–57, 2014

standard. Before 1991, the calibration data for each sensor were fit to the equation proposed by Swartz (1954),

$$\mathcal{T} = \frac{a_0}{a_1 + \log R_s} - a_2 \tag{6}$$

in the manner described by Sass et al. (1971). Using the best-fit values for the calibration constants (a_0, a_1, a_2), the sensor resistances R_s obtained during a logging experiment are converted to temperature $\mathcal{T}$.

In 1992, a multi-year effort to upgrade certain aspects of the USGS temperature calibration facility was initiated. These upgrades included a higher quality SPRT, a more sensitive and stable SPRT resistance readout, and a temperature calibration bath with a more stable and uniform temperature field that was also capable of reaching much colder temperatures (−60 °C). In conjunction with these changes, the calibration function used to fit the higher quality data was changed to,

$$\mathcal{T}^{-1} = a_0 + a_1(\ln R_s) + a_2(\ln R_s)^2 + a_3(\ln R_s)^3, \tag{7}$$

where a_0, a_1, a_2, and a_3 are now the calibration constants and $\mathcal{T}$ is expressed in Kelvin. This 4-term function offered a more precise fit to the calibration data, particularly below 0 °C. Equation (7) is an extension of the often used 3-term Steinhart–Hart equation (Steinhart and Hart, 1968) which proved inadequate for our purposes. Figure 6 shows sample calibration data and the resulting 4-term calibration fit for one of the USGS temperature sensors.

2.2.3 Denoising

Since the deconvolution step amplifies noise by up to an order of magnitude at periods less than 3–4 probe time constants (45–60 s for the DOI/GTN-P borehole records), it is essential to remove as much of the high- and mid-frequency noise as possible before attempting to deconvolve the data. Three different types of noise need to be considered for the DOI/GTN-P temperature records: (1) outliers due to a sudden change in

ESSDD
7, 1–57, 2014
Temperature data from the DOI/GTN-P Deep Borehole Array
G. D. Clow

the electric field surrounding the measuring circuit (pre-1999 measurements), (2) instrumental noise, and (3) rapid temperature oscillations due to convection of the borehole fluid. An important consideration is that the frequency content of the climate signal present in these temperature records changes with depth. In addition, the magnitude and frequency of borehole convective noise is sensitive to the temperature gradient $\partial T/\partial z$ and thus also changes with depth. Given the nature of the signal and the noise, simple band-pass filtering cannot be used to remove the noise while still preserving the essence of the climate signal.

For the DOI/GTN-P borehole temperature measurements, denoising is accomplished using a discrete wavelet analysis (Strang and Nguyen, 1996). Wavelet denoising allows thresholds to be set so that a real signal rising above the noise can be preserved while noise is removed, even if they occur at the same frequency. Given the smooth nature of the underlying temperature signal, order-3 Coiflets were selected for the analyzing wavelets; these wavelets appear ideal for this purpose, being relatively smooth and nearly symmetric. Wavelet denoising was performed at spatial scales finer than 3.4 m (periods $\leq$ 64 s) for the post-1991 logs, and finer than 5.0 m for the earlier continuous logs. The top and bottom of the logs were extended slightly to minimize border distortion. During the first pass through the wavelet denoising, data points more than 3.5 standard deviations from the smooth denoised signal are identified as outliers and removed. As the outliers may have distorted the denoised signal on the first pass, the outlier-free data are passed through the wavelet denoising a second time. Figure 7 shows the temperature measurements and resulting denoised signal from a portion of a representative DOI/GTN-P temperature log.

Incrementally obtained temperature logs (pre-1984) were not denoised as they contain insufficient information to perform the kind of denoising analysis described above. In addition, noise amplification during the deconvolution step is not a concern since these logs do not require a temporal deconvolution.

2.2.4 Deconvolution

The USGS temperature probes have a time constant τ of 7–15 s, depending on the thermophysical properties of the fluid filling the borehole. Since τ is greater than the sampling rate (2 s), a measurement represents an average of what the probe has experienced during the last few time constants. More exactly, the temperature measurements $\mathcal{T}$ are given by the convolution of the actual temperatures in the borehole (T) with the logging system's impulse response function $h(t)$,

$$\mathcal{T}(t) = \int_{-\infty}^{\infty} h(t-\mu)T(\mu)d\mu. \tag{8}$$

Given the low capacitance of the system's measurement circuit, the system response is dominated by the characteristics of the temperature probe. Following Nielsen and Balling (1984), the impulse response function is taken to be,

$$h(t) = \begin{cases} 0, & t < t_\mathrm{o} \\ \frac{1}{\tau}\exp\left(-\frac{t-t_\mathrm{o}}{\tau}\right), & t \geq t_\mathrm{o} \end{cases} \tag{9}$$

where t_o is the time delay before the system begins to sense a temperature change. Time constant experiments with the USGS temperature sensors indicate t_o is much less than the sampling rate (Saltus and Clow, 1994).

Recognizing that a temperature log is a finite-length discrete sampling of the actual temperatures in a borehole, Eq. (8) can be approximated by the summation,

$$\mathcal{T}_i = \sum_{j=1}^{n} h_j T_{i-j+1} \tag{10}$$

where n is the number of terms in the response function h. Using serial division, Eq. (10) can be inverted to find the actual borehole temperatures in terms of the mea-

ESSDD
7, 1–57, 2014

surements (Saltus and Clow, 1994),

$$T_i = \frac{\mathcal{T}_i - \sum_{j=1}^{n-1} h_{j+1} T_{i-j}}{h_1}, \quad i \geq 2. \tag{11}$$

Beginning in 1991, the temperature sensor was always allowed to reach thermal equilibrium at a fixed depth in the borehole fluid before beginning to move the sensor downhole. In this case, the first value T_1 is equal to the measured value $\mathcal{T}_1$ and we can take $T_{i-j} = \mathcal{T}_1$ when $(i-j) \leq 0$ in Eq. (11). This procedure was generally not used for the pre-1991 temperature logs. Rather, the temperature sensor was lowered from the surface into the borehole fluid without pausing. The deconvolution errors for the first 60 s (3–4 τ) of these logs are quite large. Hence, the upper few meters of the 1984–1991 logs are discarded. Returning to Fig. 7, we can see the relationship between the actual temperatures in a borehole (deconvolved signal) and the measurements obtained by the logging system for a sample DOI/GTN-P temperature log.

3 DOI/GTN-P borehole temperatures

3.1 Temperature-depth profiles

The processed temperature-depth profiles $T(z)$ derived from the 1973–2013 DOI/GTN-P borehole logs are shown in Figs. 8–30. Digital versions of the temperature profiles are available from the ACADIS repository (http://dx.doi.org/10.5065/D6N014HK). Gaps apparent in some of the profiles are almost entirely due to logging tool hangups. These occur when the temperature sensor temporarily "hangs" on a borehole casing weld or other minor obstruction and then subsequently slips by. Due to the sensor's relatively long time constant and uncertainties regarding the sensor's actual location during these hangups, it is difficult to recover the true well temperatures at these locations. The data are masked in these sections to avoid reporting erroneous values. Since the focus of

ESSDD
7, 1–57, 2014

current well-monitoring efforts is to capture climate change effects, the more recent temperature logs are generally made only to ∼ 200 m as little temperature change is expected beyond this depth.

3.2 Drilling disturbance

The DOI/GTN-P monitoring wells were drilled using conventional rotary drilling techniques. In the process, a drilling fluid is pumped downhole through the drill pipe to the bottom of the well to pick up the drill cuttings for return to the surface via the annulus between the drill pipe and the borehole wall. As a result, heat is exchanged between the circulating drill fluid and the borehole wall at a rate that depends on their relative temperature difference and the physical properties of the two media. As the fluid tends to take on the average temperature of the rock column penetrated by the borehole, the net effect is to cool the lower portion of a deep borehole while the upper portion warms. After cessation of drilling, temperatures in the well and surrounding rock gradually return to the undisturbed predrilling condition. As these wells were drilled to much greater depths (up to 6 km) than the portion that has remained accessible for temperature logging, all the logs were acquired from the upper zone that was warmed by drilling. As a result, the DOI/GTN-P temperature profiles exhibit a gradual cooling over time (left panels, Figs. 8–30).

Although the transfer of heat within a well during drilling is a complicated process, the recovery of a well from the drilling disturbance can be approximated by a simple relationship for times not too soon after well completion. If t is the time since the drill bit first reached a given depth z and s is the duration of the drilling disturbance at that depth (i.e., the duration of fluid circulation), then the temperature at depth z and time t can be approximated by,

$$T(z,t) = T_o(z) + \frac{\bar{q}_l}{4\pi K}\left[\ln\left(\frac{t}{t-s}\right) - \frac{a^2}{2\kappa s}\left(\frac{s}{t}\right)^2 + O\left(\frac{s}{t}\right)^3\right] \tag{12}$$

ESSDD
7, 1–57, 2014

where $T_o(z)$ is the undisturbed predrilling temperature, K is the thermal conductivity of the surrounding rock, κ is the rock's thermal diffusivity, a is the borehole radius, and $\bar{q}_l$ is the mean heat-flux from the drilling fluid into the surrounding rock per unit length of borehole (Lachenbruch and Brewer, 1959). The validity of this expression is restricted to times $t \gg s$. If we let $\tau \equiv (t/s)$ represent dimensionless time, Eq. (12) can be re-expressed as,

$$T(z,\tau) = T_o(z) + \frac{\bar{q}_l}{4\pi K}\left[\ln\left(1+\frac{1}{\tau}\right) - \frac{1}{2F_s\tau^2} + O(\tau^{-3})\right] \tag{13}$$

where $F_s \equiv (\kappa s/a^2)$ is the dimensionless source-function Fourier number. For the DOI/GTN-P temperature logs, τ is large enough that the term of order τ^{-3} is negligible and can be ignored. The second term in brackets takes into account the finite dimension of a well and is only important when the product $F_s\tau^2$ is small. Most of the DOI/GTN-P monitoring wells were drilled over a few months and have associated Fourier numbers F_s in the range 100–300 while the remaining wells took roughly a year to drill and have F_s values exceeding 1500. Given these large Fourier numbers, the second term in brackets (Eq. 13) is small and can be safely ignored under the conditions for which the equation is valid ($t \gg s$).

Figure 31 shows the recovery of temperatures from the drilling disturbance in one of the DOI/GTN-P monitoring wells (Atigaru Test Well No. 1). The temperatures do indeed recover in the manner predicted by Eq. (13) for $\tau > 8$. The right panel of Fig. 31 shows the evolution of the thermal drilling disturbance,

$$\Delta T_d(z,\tau) = T(z,\tau) - T_o(z) \tag{14}$$

over time. For the last log obtained in the Atigaru well (13 August 2007), the drilling disturbance had dissipated to the extent that temperatures were within 0.03–0.05 K of the undisturbed predrilling condition. Table 2 lists the drilling disturbance values (ΔT_d) for all the DOI/GTN-P wells during the 1989, 2002–2003, 2007–2008, and 2012–2013 field campaigns. With the exception of the Tunalik test well, the drilling disturbances remaining in the DOI/GTN-P monitoring wells were of order 0.1 K or less by the early 2000s. For all but five of the wells (AWU, LBN, NIN, SBE, TLK), ΔT_d was of order 0.1 K or less substantially earlier (i.e., by 1989).

3.3 Latent heat effects

Many of the wells display an abnormally slow recovery for intervals within the permafrost layer, particularly at small dimensionless times τ. The J. W. Dalton and Seabee test wells are good examples (Figs. 15 and 24), as is the 250 m depth in the Atigaru well (Fig. 8). This slow recovery is attributable to latent heat effects. While drilling a deep borehole through permafrost, interstitial ice within the permafrost zone generally thaws in the vicinity of the well. Once the well is completed, the thawed interstitial ice releases its latent heat upon refreezing, retarding the cooling process as the permafrost returns to its predrilling state. Permafrost intervals showing a delayed recovery are likely to have appreciable amounts of interstitial ice. An extensive discussion of latent heat effects in permafrost can be found in Lachenbruch et al. (1982).

3.4 Temperature gradients

Temperature gradients $\partial T/\partial z$ calculated from select temperature profiles are shown in the right panels of Figs. 8–30 for all of the DOI/GTN-P monitoring wells. Except for the upper 100 m where climate-change effects are large, the gradients primarily reflect thermal conductivity variations with depth; thermal profiles undisturbed by latent heat effects were used wherever possible to find the gradients. A 10 m averaging interval was used for the gradient calculations, 2–3 times greater than the spatial scales at which the wavelet denoising and deconvolution operate. In most cases, the thermal gradient determined in this way shows good agreement among logs for any given well. Depths below 100 m where the gradient $\partial T/\partial z$ between logs is disparate indicate intervals where one or more of the temperature profiles is less certain. Unlike nearby

ESSDD
7, 1–57, 2014

Prudhoe Bay, a significant change in the temperature gradient is not observed at the base of permafrost in the NPR-A wells or in the Lupine or Echooka test wells; the strong gradient contrast at the base of permafrost in Prudhoe Bay has been attributed to the high porosity (~ 39 %) of the saturated coarse-grained materials found there (Lachenbruch et al., 1982).

3.5 Borehole fluid convection

The fluid in a monitoring well is expected to freely convect wherever the temperature gradient exceeds a value given by the sum of a lapse rate term and the critical potential-temperature gradient,

$$\frac{\partial T}{\partial z} > \frac{g\alpha T}{c_\mathrm{p}} + \left(\frac{\partial \theta}{\partial z}\right)_\mathrm{crit}. \tag{15}$$

Here, α is the coefficient of thermal expansion for the borehole fluid, c_p is its specific heat, g is the gravitational acceleration, and T is temperature expressed in Kelvin. The critical potential-temperature gradient,

$$\left(\frac{\partial \theta}{\partial z}\right)_\mathrm{crit} = \frac{\nu\kappa}{\alpha g a^4}\left(Ra_\mathrm{c}\gamma^4\right), \tag{16}$$

accounts for the effects of viscous drag within the fluid and the boundary conditions at the wall of the borehole; ν is the kinematic viscosity of the fluid, κ is its thermal diffusivity, a is the borehole radius, $\gamma \equiv (a/L)$ is the aspect ratio for convective cells of height L, and Ra_c is the critical Rayleigh number. Charlson and Sani (1970, 1971) found that the minimum $(Ra_\mathrm{c}\gamma^4)$ value at which convection will occur is 71 for perfectly insulating side walls and 220 for perfectly conducting walls. Using the thermal properties of the DOI/GTN-P borehole fluid (diesel oil), the radius of the boreholes (12–17 cm), and assuming thermally conducting sidewalls (a reasonable assumption for these wells), the lapse rate term is 1.44 $\mathrm{mK\,m^{-1}}$ while the critical potential-temperature gradient is much

ESSDD
7, 1–57, 2014

smaller, 0.007–0.028 $\mathrm{mK\,m^{-1}}$. Thus, the viscosity of the fluid and resistive drag on the walls is small enough that the onset of convection in these wells is predominantly determined by the lapse rate term. Considering both terms, free convection is expected to occur at all depths where the temperature gradient exceeds 1.47 $\mathrm{mK\,m^{-1}}$. Except for the climate-induced gradient reversal near the surface, the temperature gradients in these wells exceed the value necessary for the onset of convection by more than an order of magnitude. Thus the form of the convective flow is expected to be fully turbulent. Analysis of the temperature logs confirms that the borehole fluid is undergoing turbulent convection. Random temperature fluctuations as large as ±10 mK associated with the turbulent eddies constitutes the primary source of noise in the post-1999 temperature logs.

During the spring and early summer, temperature gradients typically exceed 100 $\mathrm{mK\,m^{-1}}$ in the upper ∼ 10 m of permafrost. As a result, convection of the borehole fluid can become so intense that the temperatures within the monitoring wells become nearly isothermal during this period at shallow depths. Figure 32 shows temperatures in the Koluktak test well monitored by a thermistor string located 5–13 m below the surface. Strong positive temperature gradients develop near-surface by early March as the permafrost chills. By early June, the isothermal zone extends down to 10 m in this well and then warms in response to summer heating. By early- to mid-August, near-surface gradients weaken, shallow convection ceases, and the isothermal zone vanishes. As most of the DOI/GTN-P temperature logs have been acquired at about the convective transition period, many of the logs show an isothermal section in the upper ∼ 10 m while others do not.

3.6 Climate change effects

Although the temperatures in this dataset have not been corrected for the thermal drilling disturbance, measurements acquired during the last 25 yr when the disturbance has been small demonstrate the magnitude of permafrost warming experienced on the

ESSDD
7, 1–57, 2014

Arctic Slope of Alaska since the late 1980s. Figure 33 shows the last four temperature logs acquired in the Awuna test well as an example. Correcting the logs for the drilling disturbance is a high priority as it will give a clearer picture of how near-surface temperatures in permafrost have evolved in this region since the onset of the monitoring program in 1973.

4 Summary

A 40 yr dataset of borehole temperature measurements from continuous permafrost in arctic Alaska has been assembled for the period 1973–2013. The data represent the true temperatures in the wellbores and surrounding rocks at the time of the measurements; they have not been corrected to remove the thermal disturbance caused by drilling the wells. With a few exceptions, the drilling disturbance is estimated to have been of order 0.1 K or less by 1989. Thus, most of the temperature measurements acquired during the last 25 yr are little affected by the drilling disturbance. The data contribute to ongoing efforts to monitor changes in the thermal state of permafrost in both hemispheres by the Global Terrestrial Network for Permafrost (GTN-P), one of the primary subnetworks of the Global Terrestrial Observing System (GTOS). In addition, the data will be useful for refining our basic understanding of the physical conditions in near-surface materials on the Arctic Slope of Alaska, including the thickness of permafrost and its ice content, as well as provide important information for validating predictive models used for climate impact assessments. The dataset may also prove useful for testing the validity of borehole recovery models used to describe how the thermal disturbance caused by drilling diminishes over time. Such models are often used to ascertain undisturbed rock temperatures from a series of temperature logs perturbed by drilling effects. Very few high-quality datasets are available for testing such models, particularly in permafrost terrain. The fully processed borehole temperature data are available online from the ACADIS repository at doi:10.5065/D6N014HK.

ESSDD
7, 1–57, 2014

Acknowledgements. We gratefully acknowledge funding support from a number of USGS programs that have made acquisition of this dataset possible over the years, including: the Earthquakes, Volcanoes, and Engineering Program, the Earth System Dynamics Program, and most recently the Climate and Land Use Change Program. Logistics support from BLM's Arctic District Office has been greatly appreciated. Special thanks goes to John Kennelly and Mark Ohms whose expertise has kept the instrumentation running, and especially to Art Lachenbruch for his insight regarding the potential for extracting climate information from permafrost temperature profiles. Any use of trade, firm, or product names is for descriptive purposes only and does not imply endorsement by the US Government.

References

Beltrami, H. and Mareschal, J. C.: Ground temperature histories for central and eastern Canada from geothermal measurements: Little Ice Age signature, Geophys. Res. Lett., 19, 689–692, 1992. 4

Charlson, G. S. and Sani, R. L.: Thermoconvective instability in a bounded cylindrical fluid, Int. J. Heat Mass Transfer, 13, 1479–1496, 1970. 17

Charlson, G. S. and Sani, R. L.: On thermoconvective instability in a bounded cylindrical fluid layer, Int. J. Heat Mass Transfer, 14, 2157–2160, 1971. 17

Clow, G. D.: USGS Polar Temperature Logging System, Description and Measurement Uncertainties, US Geological Survey, Reston, Virginia USA, Techniques and Methods 2–E3, available at: http://pubs.usgs.gov/tm/02e03 (last access: January 2014), 24 pp., 2008. 6, 8

Clow, G. D.: USGS permafrost temperatures acquired from the DOI/GTN-P Deep Borehole Array in arctic Alaska, 1973-continuing, Advanced Cooperative Arctic Data and Information Service (ACADIS), Boulder, Colorado USA, doi:10.5065/D6N014HK, 2013.

Gryc, G.: Geology and exploration of the National Petroleum Reserve in Alaska, 1974 to 1982, Professional Paper 1399, US Geological Survey, Reston, Virginia USA, 940 pp., 1988. 3

International Permafrost Association (IPA): IPA-IPY thermal state of permafrost (TSP) snapshot borehole inventory, National Snow and Ice Data Center, Boulder, Colorado USA, doi:10.7265/N57D2S25, 2010. 5

Jeffries, M. O., Richter-Menge, J., and Overland, J. E. (Eds.): Arctic Report Card 2012, available at: http://www.arctic.noaa.gov/report12 (last access: January 2014), 2012. 2

Jeffries, M. O., Overland, J. E., and Perovich, D. K.: The Arctic shifts to a new normal, Phys. Today, 66, 35–40, 2013. 2

Lachenbruch, A. H. and Brewer, M. C.: Dissipation of the temperature effect of drilling a well in arctic Alaska, Bulletin 1083-C, US Geological Survey, Reston, Virginia USA, 73–109, 1959. 3, 15

Lachenbruch, A. H. and Marshall, B. V.: Changing climate: geothermal evidence from permafrost in the Alaskan Arctic, Science, 234, 689–696, 1986. 4

Lachenbruch, A. H., Sass, J. H., Marshall, B. V., and Moses Jr., T. H.: Permafrost, heat flow, and the geothermal regime at Prudhoe Bay, Alaska, J. Geophys. Res., 87, 9301–9316, 1982. 4, 16, 17

Lachenbruch, A. H., Sass, J. H., Lawver, L. A., Brewer, M. C., Marshall, B. V., Munroe, R. J., Kennelly, J. P., Galanis Jr., S. P., and Moses Jr., T. H.: Temperature and depth of permafrost on the Arctic Slope of Alaska, Professional Paper 1399, US Geological Survey, Reston, Virginia USA, 645–656, 1988a. 8

Lachenbruch, A. H., Cladouhos, T. T., and Saltus, R. W.: Permafrost temperature and the changing climate, in: Proceedings of the 5th International Conference on Permafrost, Trondheim, Norway, 2–5 August 1988, vol. 3, 9–17, 1988b. 4

Mareschal, J. C. and Beltrami, H.: Evidence for recent warming from perturbed geothermal gradients: examples from eastern Canada, Clim. Dynam., 6, 135–153, 1992. 4

Nielsen, S. B. and Balling, N.: Accuracy and resolution in continuous temperature logging, Tectonophysics, 103, 1–10, 1984. 12

Nielsen, S. B. and Beck, A. E.: Heat flow density values and paleoclimate determined from stochastic inversion of four temperature-depth profiles from the Superior Province of the Canadian Shield, Tectonophysics, 164, 345–359, 1989. 4

Osterkamp, T. E. and Jorgenson, J. C.: Warming of permafrost in the Arctic National Wildlife Refuge, Alaska, Permafrost Periglac., 17, 65–69, 2006. 4

Osterkamp, T. E. and Romanovsky, V. E.: Evidence for warming and thawing of discontinuous permafrost in Alaska, Permafrost Periglac., 10, 17–37, 1999. 4

Saltus, R. W. and Clow, G. D.: Deconvolution of Continuous Borehole Temperature Logs: Algorithms and Accuracies, Open-File Report 94–254, US Geological Survey, Reston, Virginia USA, 42 pp., 1994. 12, 13

Sass, J. H., Lachenbruch, A. H., Munroe, R. J., Greene, G. W., and Moses, T. H., Jr.: Heat flow in the western United States, J. Geophys. Res., 76, 6376–6413, 1971. 6, 8, 10

ESSDD
7, 1–57, 2014

Temperature data from the DOI/GTN-P Deep Borehole Array

G. D. Clow

Sessa, R. and Dolman, H. (Eds.): Terrestrial Essential Climate Variables for Climate Change Assessment, Mitigation and Adaption, GTOS 52, Global Terrestrial Observing System, Food and Agricultural Organization of the United Nations, Rome, 2008. 4

Smith, S. and Brown, J.: Assessment of the Status of the Development of the Standards for the Terrestrial Essential Climate Variables – T7 – Permafrost and Seasonally Frozen Ground, GTOS 62, Global Terrestrial Observing System, Food and Agricultural Organization of the United Nations, Rome, 2009. 4

Smith, S. L., Burgess, M. M., Risenborough, D., and Nixon, F. M.: Recent trends from Canadian permafrost thermal monitoring sites, Permafrost Periglac., 16, 19–30, 2005. 4

Steinhart, J. S. and Hart, S. R.: Calibration curves for thermistors, Deep-Sea Res., 15, 497–503, 1968. 10

Strang, G. and Nguyen, T.: Wavelets and Filter Banks, Wellesley-Cambridge Press, Wellesley, Massachusetts USA, 1996. 11

Swartz, J. H.: A geothermal measuring circuit, Science, 120, 573–574, 1954. 10

Taylor, A. E., Wang, K., Smith, S. L., Burgess, M. M., and Judge, A. S.: Canadian arctic permafrost observatories: detecting climate change through inversion of subsurface time series, J. Geophys. Res., 111, B02411, doi:10.1029/2004JB003208, 2006. 4

Urban, F. E. and Clow, G. D.: DOI/GTN-P climate and active-layer data acquired in the National Petroleum Reserve–Alaska and the Arctic National Wildlife Refuge, Data Series 812, US Geological Survey, Reston, Virginia USA, doi:10.3133/ds812, 2014. 5

ESSDD
7, 1–57, 2014
Temperature data from the DOI/GTN-P Deep Borehole Array
G. D. Clow

Table 1. USGS and GTN-P well codes, location, maximum accessible depth, and date of first temperature log for the DOI/GTN-P monitoring wells. Boreholes coupled with a nearby DOI/GTN-P climate station are indicated.

Borehole	USGS Code	GTN-P Code	Latitude (north)	Longitude (west)	Depth (m)	First Log (yr-mon-day)	Climate Station
Atigaru Test Well #1	ATI	US 01	70°33.348′	151°43.229′	648	1977 Dec 14	
Awuna Test Well #1	AWU	US 02	69°09.193′	158°01.355′	884	1981 Aug 22	•
Drew Point Test Well #1	DRP	US 03	70°52.762′	153°54.202′	640	1978 Sep 17	•
East Simpson Test Well #1	ESN	US 04	70°55.046′	154°37.286′	600	1979 Sep 13	
East Teshekpuk Test Well #1	ETK	US 05	70°34.171′	152°56.815′	727	1977 Dec 17	•
Echooka Unit #1 (Mobil Oil)	EB1	US 93	69°23.994′	148°16.313′	595	1973 Sep 26	
Ikpikpuk Test Well #1	IKP	US 07	70°27.305′	154°20.082′	615	1980 Sep 10	•
J. W. Dalton Test Well #1	JWD	US 08	70°55.207′	153°08.454′	483	1979 Sep 13	
Koluktak Test Well #1	KOL	US 10	69°45.144′	154°36.669′	227	1981 Aug 23	•
Kugrua Test Well #1	KAG	US 09	70°35.191′	158°39.923′	582	1978 Sep 15	
Kuyanak Test Well #1	KUY	US 11	70°55.869′	156°04.092′	856	1981 Aug 25	
Lisburne Test Well #1	LBN	US 12	68°29.061′	155°41.773′	532	1980 Sep 09	
Lupine Unit #1 (Forest Oil)	LUP	US 92	69°06.051′	148°37.290′	469	1975 Aug 15	
North Inigok Test Well #1	NIN	US 13	70°15.435′	152°46.139′	625	1982 Aug 31	
North Kalikpik Test Well #1	NKP	US 14	70°30.550′	152°22.070′	660	1978 Sep 16	
Peard Bay Test Well #1	PEA	US 15	70°42.939′	159°00.042′	591	1979 Sep 15	
Seabee Test Well #1	SBE	US 16	69°22.809′	152°10.522′	393	1980 Sep 09	•
South Harrison Test Well #1	SOH	US 18	70°25.468′	151°44.071′	399	1977 Dec 16	
South Meade Test Well #1	SME	US 17	70°36.872′	156°53.601′	549	1979 Sep 14	•
Tulageak Test Well #1	TUL	US 20	71°11.338′	155°44.228′	756	1981 Aug 24	
Tunalik Test Well #1	TLK	US 19	70°12.358′	161°04.153′	556	1980 Sep 15	•
West Dease Test Well #1	WDS	US 21	71°09.524′	155°37.983′	823	1980 Sep 14	
West Fish Creek Test Well #1	FCK	US 06	70°19.600′	152°03.634′	735	1977 Dec 11	•

ESSDD
7, 1–57, 2014

Table 2. Drilling disturbance ΔT_d remaining in the DOI/GTN-P monitoring wells at the time of the 1989, 2002–2003, 2007–2008, and 2012–2013 field campaigns. The corresponding dimensionless times τ are also listed.

Borehole	USGS	Drilling	1989		2002–2003		2007–2008		2012–2013	
	Code	Duration (days)	τ	ΔT_d (K)	τ	ΔT_d (K)	τ	ΔT_d (K)	τ	ΔT_d (K)
Atigaru Test Well #1	ATI	60	76	0.07–0.13	156	0.03–0.06	186	0.03–0.05	–	–
Awuna Test Well #1	AWU	412	8	0.20–0.33	20	0.09–0.14	25	0.07–0.11	29	0.06–0.10
Drew Point Test Well #1	DRP	54	78	0.05–0.09	173	0.02–0.04	200	0.02–0.04	–	–
East Simpson Test Well #1	ESN	44	87	0.07–0.11	195	0.03–0.05	236	0.03–0.04	278	0.03–0.04
East Teshekpuk Test Well #1	ETK	56	87	0.05–0.09	179	0.02–0.04	205	0.02–0.04	–	–
Echooka Unit #1	EB1	160	–	–	–	–	–	–	94	0.04–0.05
Ikpikpuk Test Well #1	IKP	442	9	0.09–0.16	20	0.04–0.07	24	0.04–0.06	28	0.03–0.05
J. W. Dalton Test Well #1	JWD	86	43	0.10–0.16	103	0.04–0.07	–	–	–	–
Koluktak Test Well #1	KOL	24	127	0.04	326	0.01–0.02	401	0.01	477	0.01
Kugrua Test Well #1	KAG	98	43	0.13–0.16	91	0.06–0.07	113	0.05–0.06	129	0.04–0.05
Kuyanak Test Well #1	KUY	42	–	–	186	0.03–0.05	229	0.03–0.04	273	0.02–0.03
Lisburne Test Well #1	LBN	344	11	0.35–0.40	25	0.12–0.18	–	–	–	–
Lupine Unit #1	LUP	309	–	–	–	–	–	–	46	0.07-0.09
North Inigok Test Well #1	NIN	45	68	0.33–0.38	175	0.13–0.15	215	0.10–0.12	256	0.09–0.10
North Kalikpik Test Well #1	NKP	40	–	–	233	0.04–0.05	269	0.03–0.04	315	0.03
Peard Bay Test Well #1	PEA	73	53	0.10–0.11	123	0.04–0.05	143	0.04	168	0.03
Seabee Test Well #1	SBE	257	14	0.19–0.26	33	0.08–0.11	40	0.07–0.09	47	0.06–0.08
South Harrison Test Well #1	SOH	67	69	0.14–0.15	140	0.07–0.08	167	0.06	195	0.05
South Meade Test Well #1	SME	341	–	–	26	0.06–0.11	32	0.05–0.09	37	0.04–0.08
Tulageak Test Well #1	TUL	22	140	0.03–0.05	373	0.01–0.02	439	0.01	–	–
Tunalik Test Well #1	TLK	407	10	0.53–0.67	22	0.24–0.29	26	0.20–0.26	30	0.17–0.22
West Dease Test Well #1	WDS	36	96	0.05–0.08	–	–	–	–	–	–
West Fish Creek Test Well #1	FCK	67	68	0.15–0.16	–	–	171	0.06	193	0.05–0.06

ESSDD
7, 1–57, 2014

Temperature data from the DOI/GTN-P Deep Borehole Array

G. D. Clow

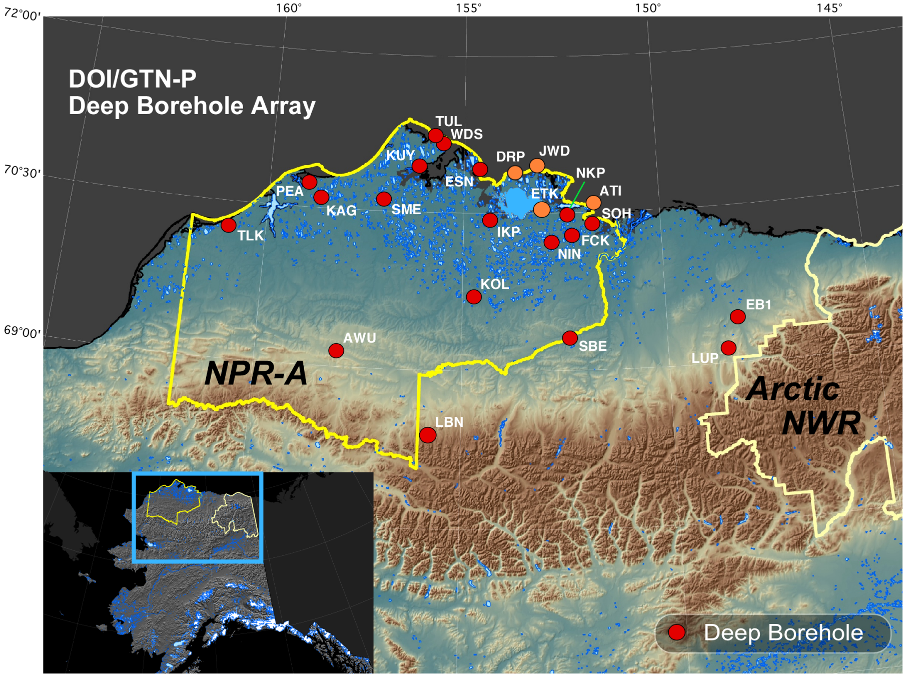

Fig. 1. Location of the 23 DOI/GTN-P boreholes used to monitor the thermal state of permafrost (TSP) in the National Petroleum Reserve–Alaska (NPR-A) and near the Arctic National Wildlife Refuge. Wells indicated by orange symbols have been plugged and are no longer accessible.

ESSDD
7, 1–57, 2014
Temperature data from the DOI/GTN-P Deep Borehole Array
G. D. Clow

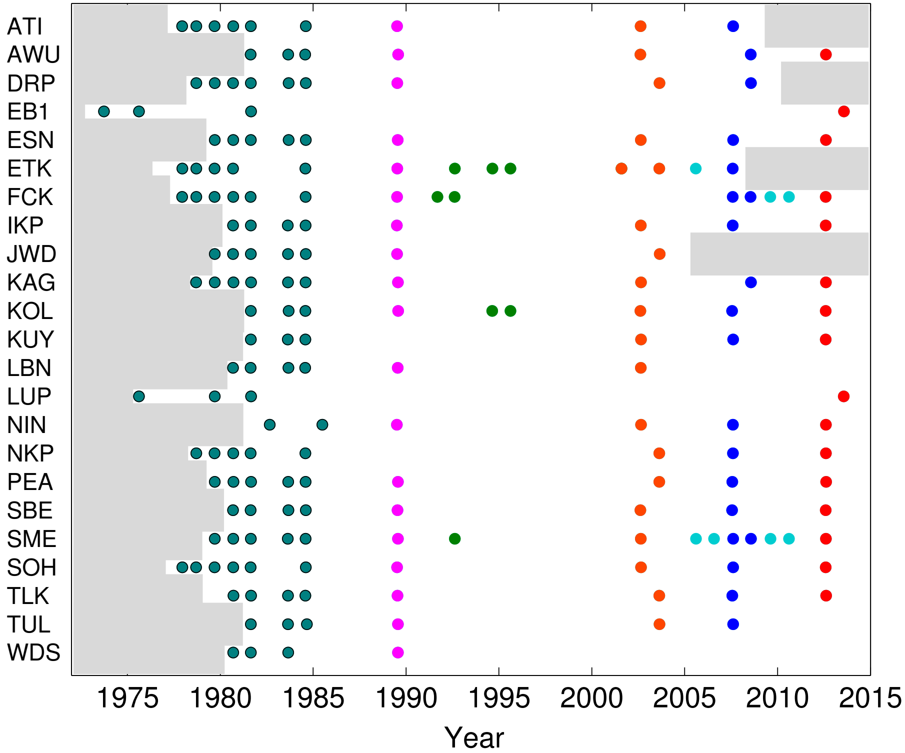

Fig. 2. Temperature logging history for the DOI/GTN-P Deep Borehole Array. Major field campaigns occurred during 1977–1984 (teal), 1989 (magenta), 2002–2003 (orange-red), 2007–2008 (blue), and 2012–2013 (red). Gray areas indicate times before well completion, and in some instances when the wells have been plugged and abandoned due to coastal erosion issues.

ESSDD
7, 1–57, 2014

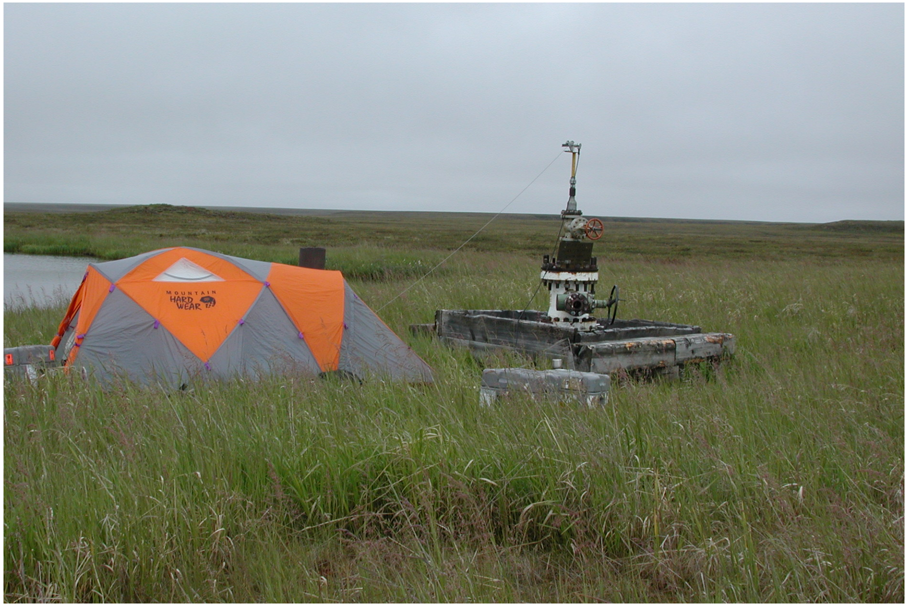

Fig. 3. Measuring temperatures in the Koluktak (KOL) Test Well No. 1, National Petroleum Reserve–Alaska. This well is typical of the other wells in the DOI/GTN-P Borehole Array.

ESSDD
7, 1–57, 2014

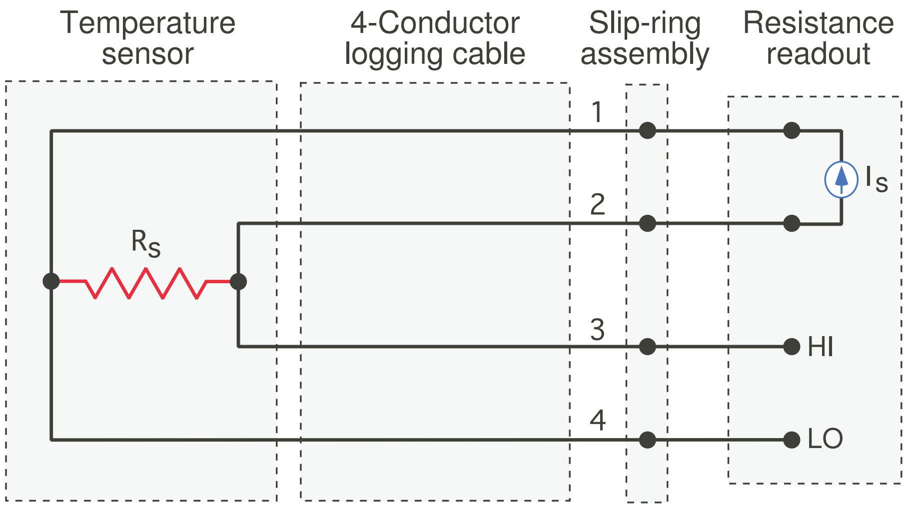

Fig. 4. Kelvin (4-wire) resistance circuit used by the USGS portable logging system. The test current I_s passes through lines 1 and 2 while the voltage drop across the probe resistance R_s is measured using the sense lines (3, 4). Logging cables used with the portable system are 450–900 m long. The resistance readout is located on the surface.

ESSDD
7, 1–57, 2014

Temperature data from the DOI/GTN-P Deep Borehole Array

G. D. Clow

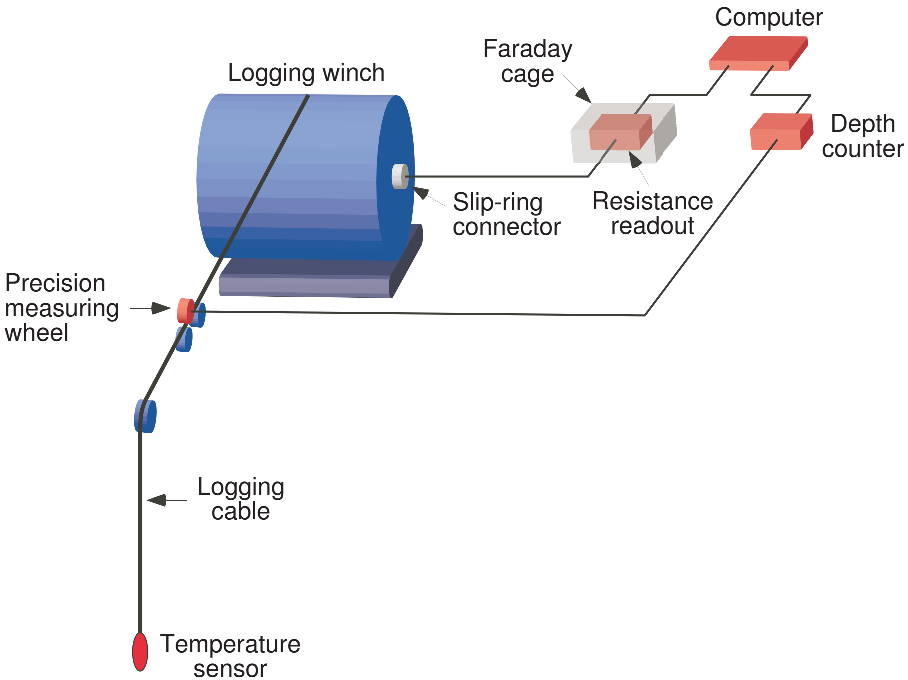

Fig. 5. Layout of the post-1999 version of the USGS portable temperature logging system used in arctic Alaska.

ESSDD
7, 1–57, 2014

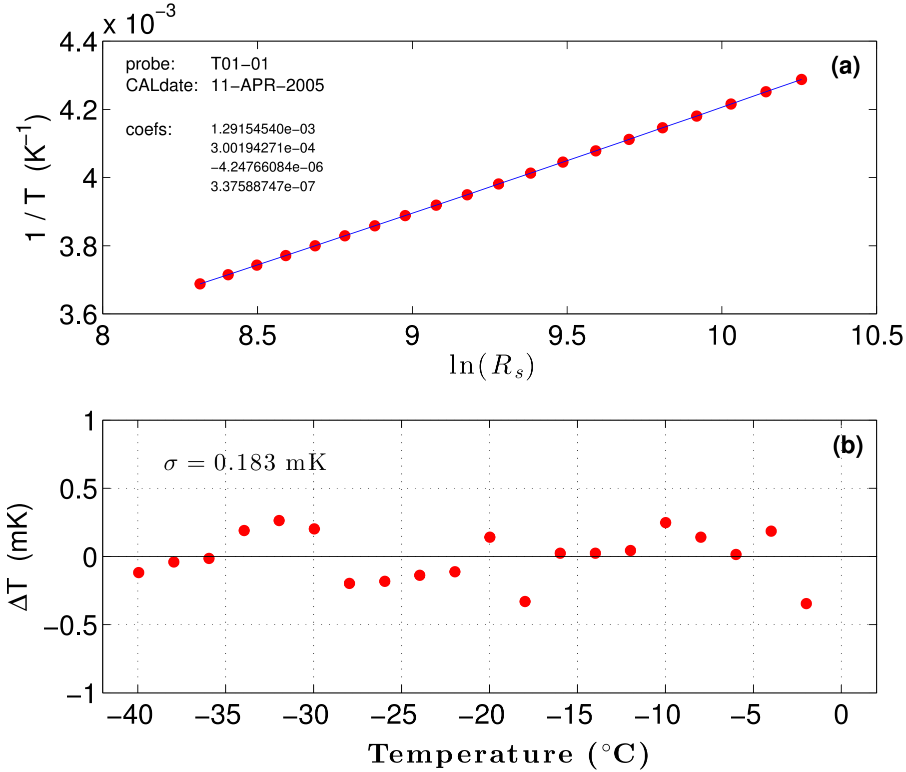

Fig. 6. Sample calibration data over the range −40 to −2 °C for one of the USGS temperature sensors (T01-01) along with the best-fit 4-term calibration function **(a)**. Panel **(b)** shows the residuals from the calibration fit. In this example, the standard deviation of the calibration residuals is 0.183 mK.

ESSDD
7, 1–57, 2014

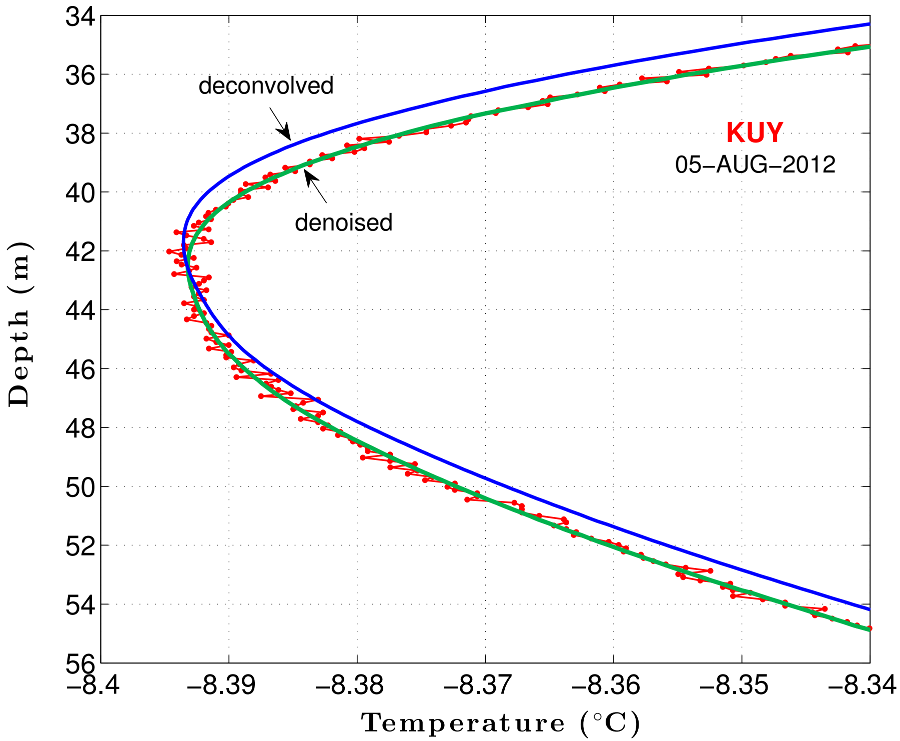

Fig. 7. Portion of a sample DOI/GTN-P temperature log (Kuyanak Test Well #1, 5 August 2012). The temperature measurements $\mathcal{T}$ are shown in red while the denoised signal is given by the green line. Blue line shows the deconvolved signal, which represents the actual temperatures T in the borehole taking into account the response time of the moving probe.

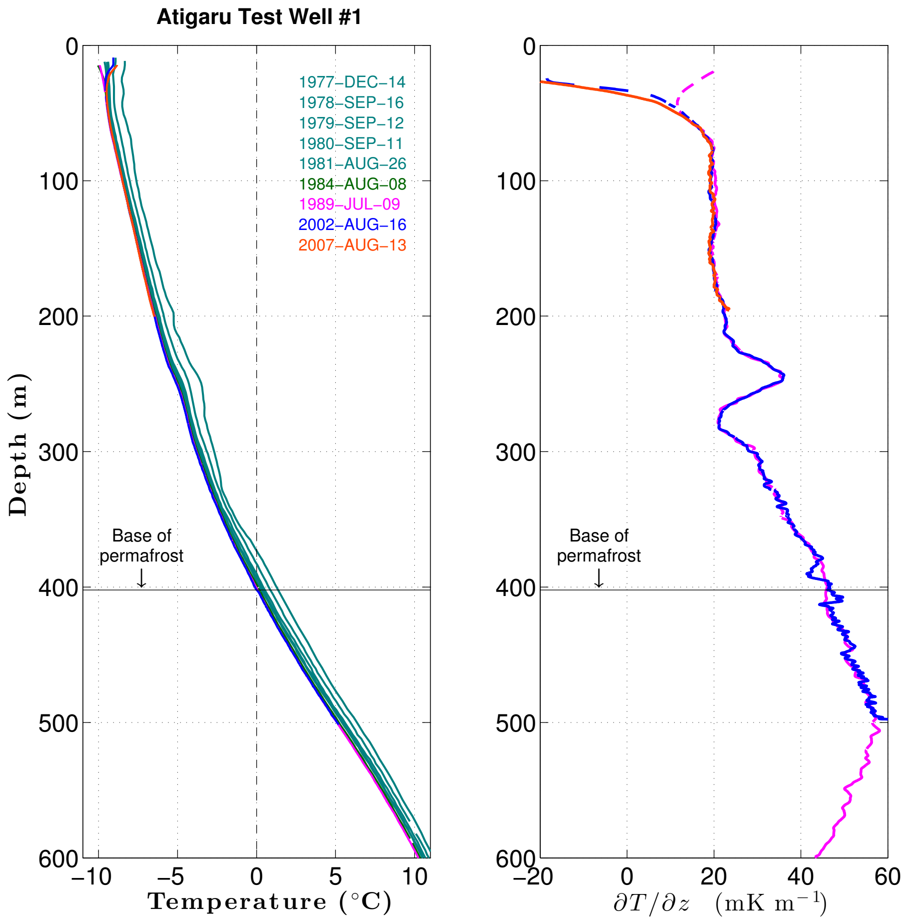

Fig. 8. Temperature profiles in the Atigaru Test Well No. 1, color-coded by acquisition date (left). Temperature gradients calculated from the 1989, 2002, and 2007 logs are shown in the right panel using the same color coding. Black horizontal line shows the base of permafrost.

ESSDD
7, 1–57, 2014

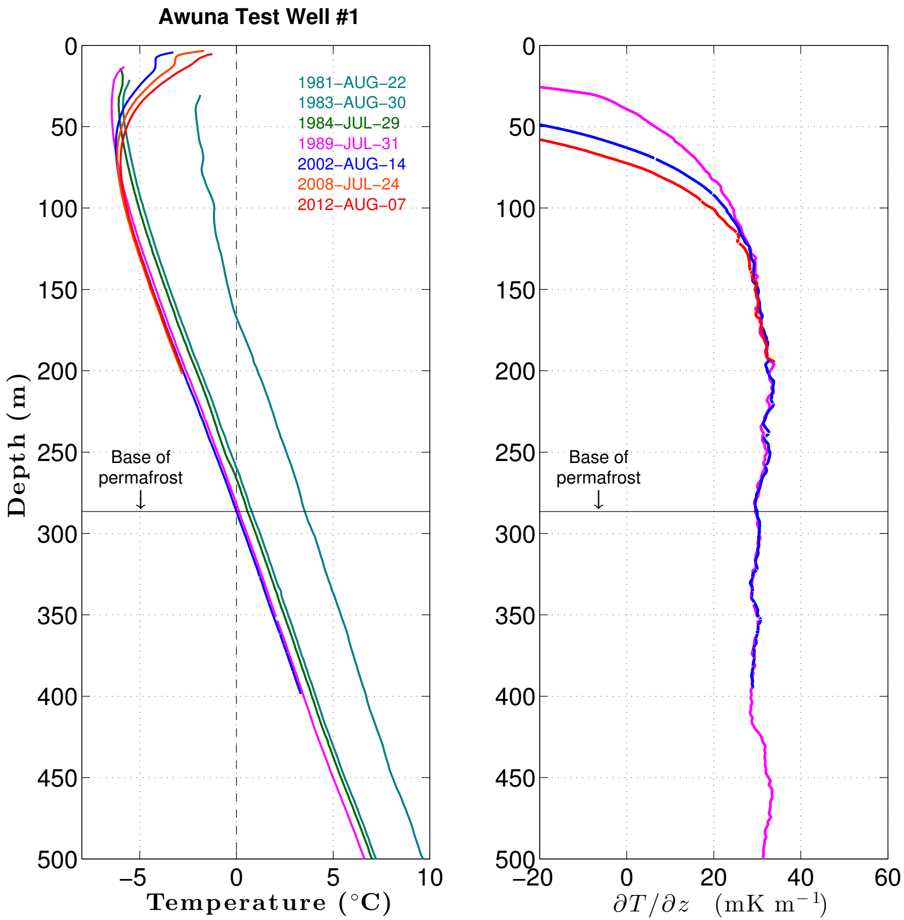

Fig. 9. Temperature profiles in the Awuna Test Well No. 1, color-coded by acquisition date (left). Temperature gradients calculated from the 1989, 2002, and 2012 logs are shown in the right panel.

ESSDD
7, 1–57, 2014

Temperature data from the DOI/GTN-P Deep Borehole Array

G. D. Clow

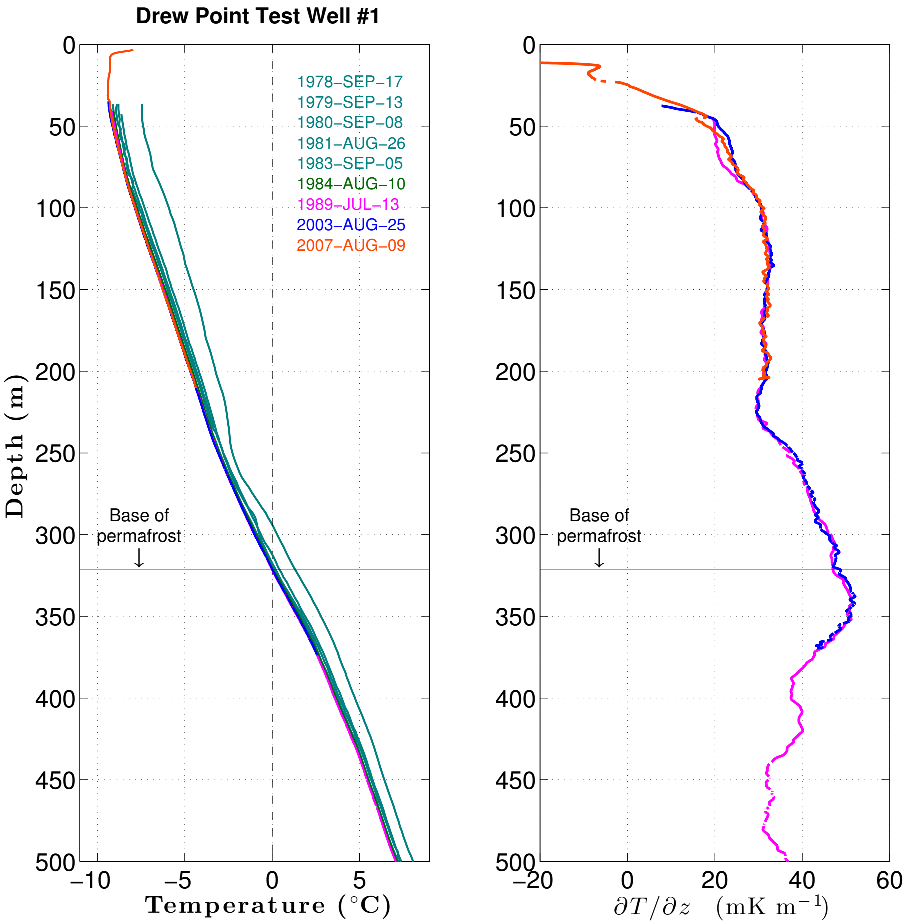

Fig. 10. Temperature profiles in the Drew Point Test Well No. 1, color-coded by acquisition date (left). Temperature gradients calculated from the 1989, 2003, and 2007 logs are shown in the right panel.

Discussion Paper | Discussion Paper | Discussion Paper | Discussion Paper |

ESSDD

7, 1–57, 2014

Temperature data from the DOI/GTN-P Deep Borehole Array

G. D. Clow

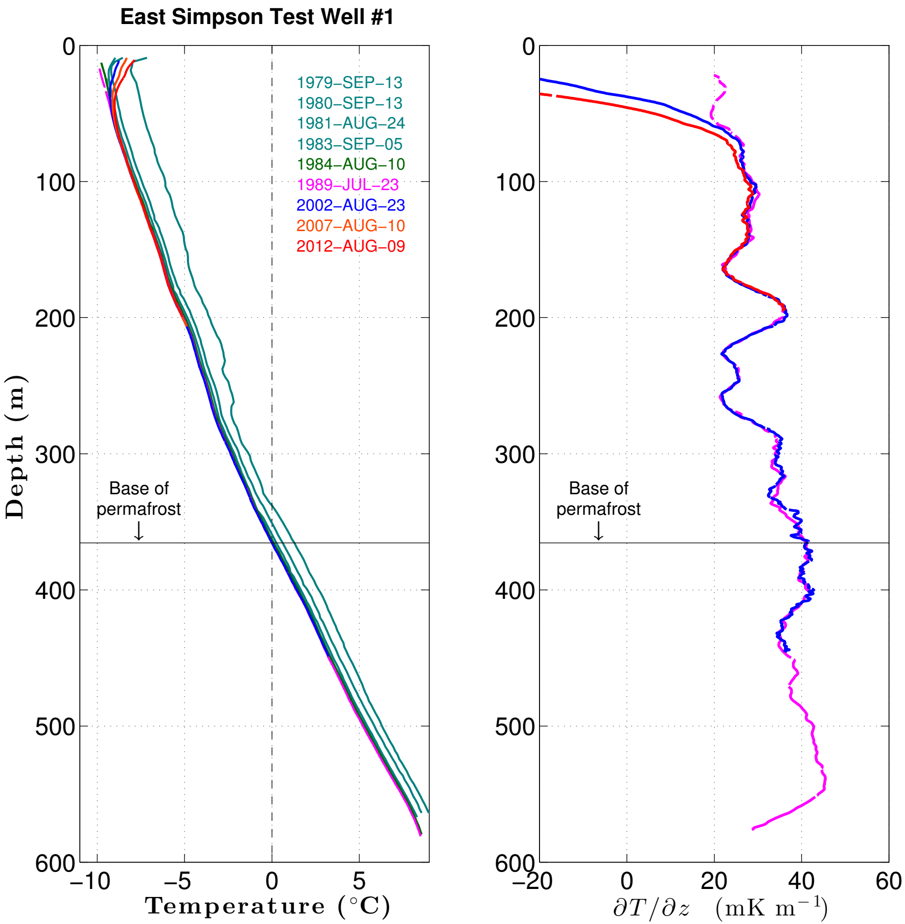

Fig. 11. Temperature profiles in the East Simpson Test Well No. 1, color-coded by acquisition date (left). Temperature gradients calculated from the 1989, 2002, and 2012 logs are shown in the right panel.

ESSDD
7, 1–57, 2014

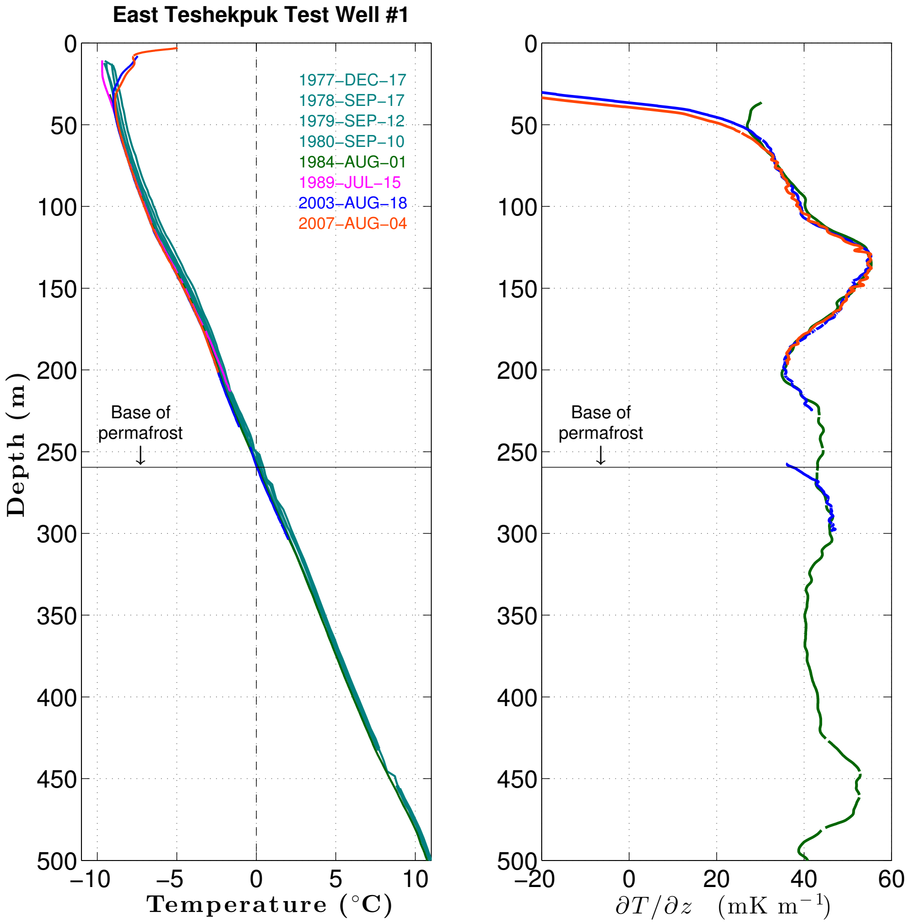

Fig. 12. Temperature profiles in the East Teshekpuk Test Well No. 1, color-coded by acquisition date (left). Temperature gradients calculated from the 1984, 2003, and 2007 logs are shown in the right panel.

ESSDD
7, 1–57, 2014

Temperature data from the DOI/GTN-P Deep Borehole Array

G. D. Clow

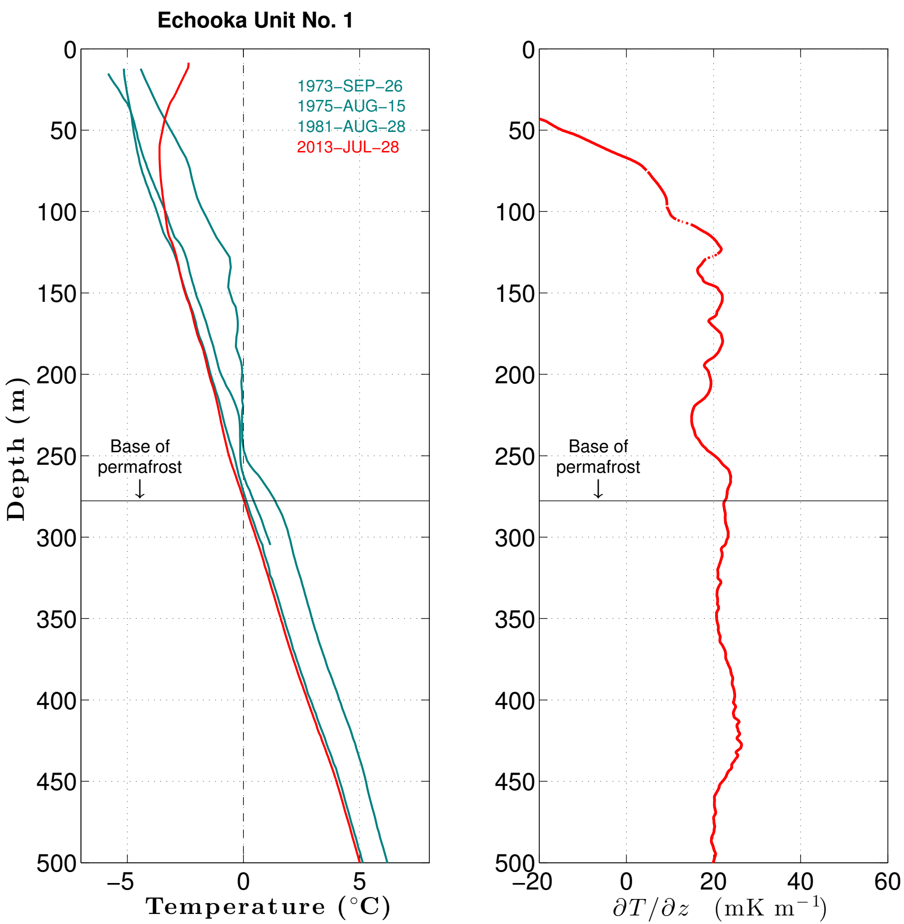

Fig. 13. Temperature profiles in the Echooka Unit No. 1 well, color-coded by acquisition date (left). The temperature gradient calculated from the 2013 log is shown in the right panel.

ESSDD
7, 1–57, 2014

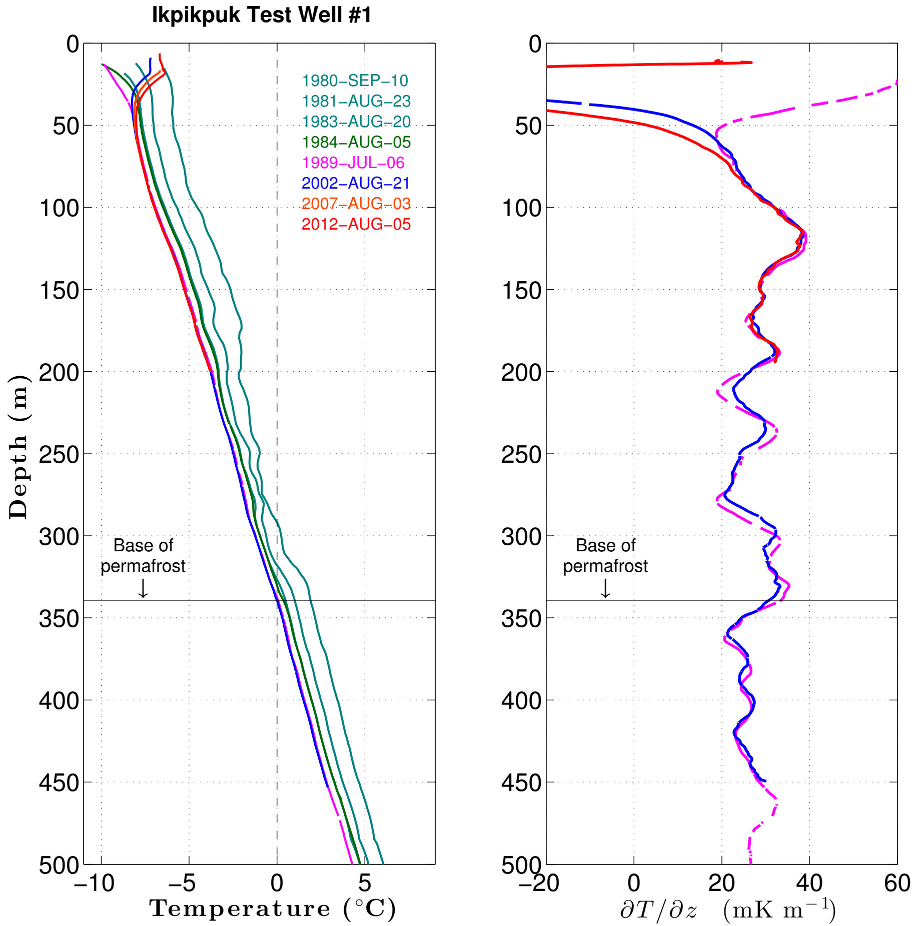

Fig. 14. Temperature profiles in the Ikpikpuk Test Well No. 1, color-coded by acquisition date (left). Temperature gradients calculated from the 1989, 2002, and 2012 logs are shown in the right panel.

ESSDD
7, 1–57, 2014

Temperature data from the DOI/GTN-P Deep Borehole Array

G. D. Clow

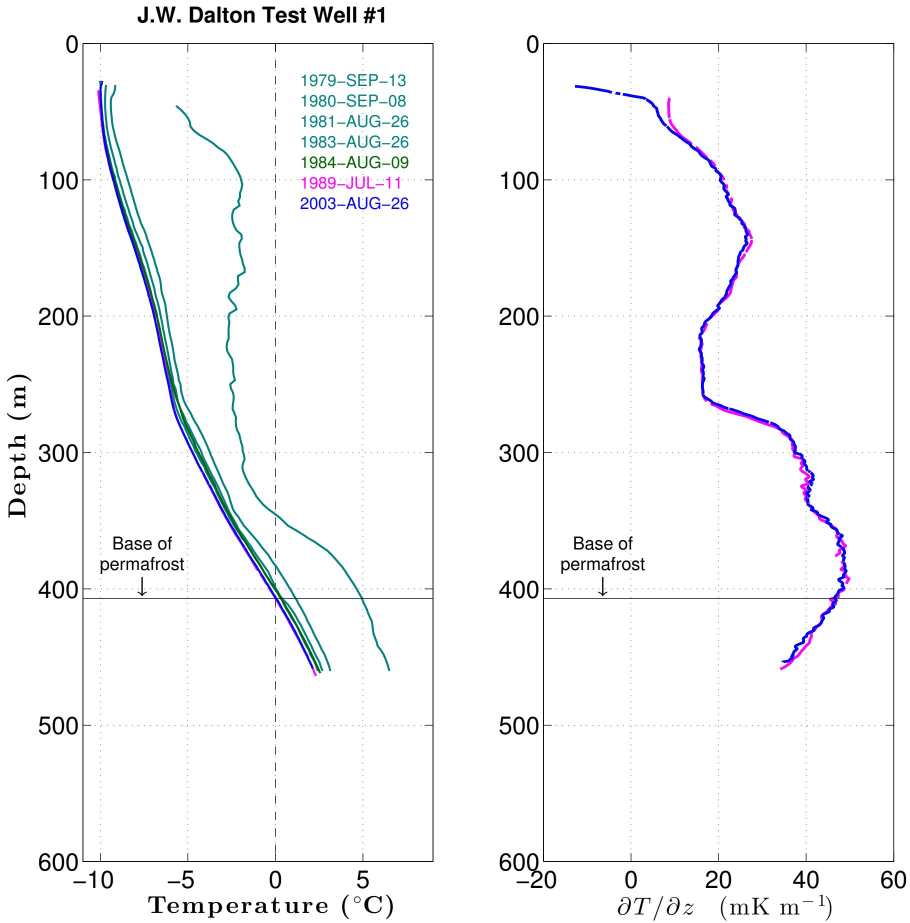

Fig. 15. Temperature profiles in the J. W. Dalton Test Well No. 1, color-coded by acquisition date (left). Temperature gradients calculated from the 1989 and 2003 logs are shown in the right panel.

ESSDD
7, 1–57, 2014

Temperature data from the DOI/GTN-P Deep Borehole Array

G. D. Clow

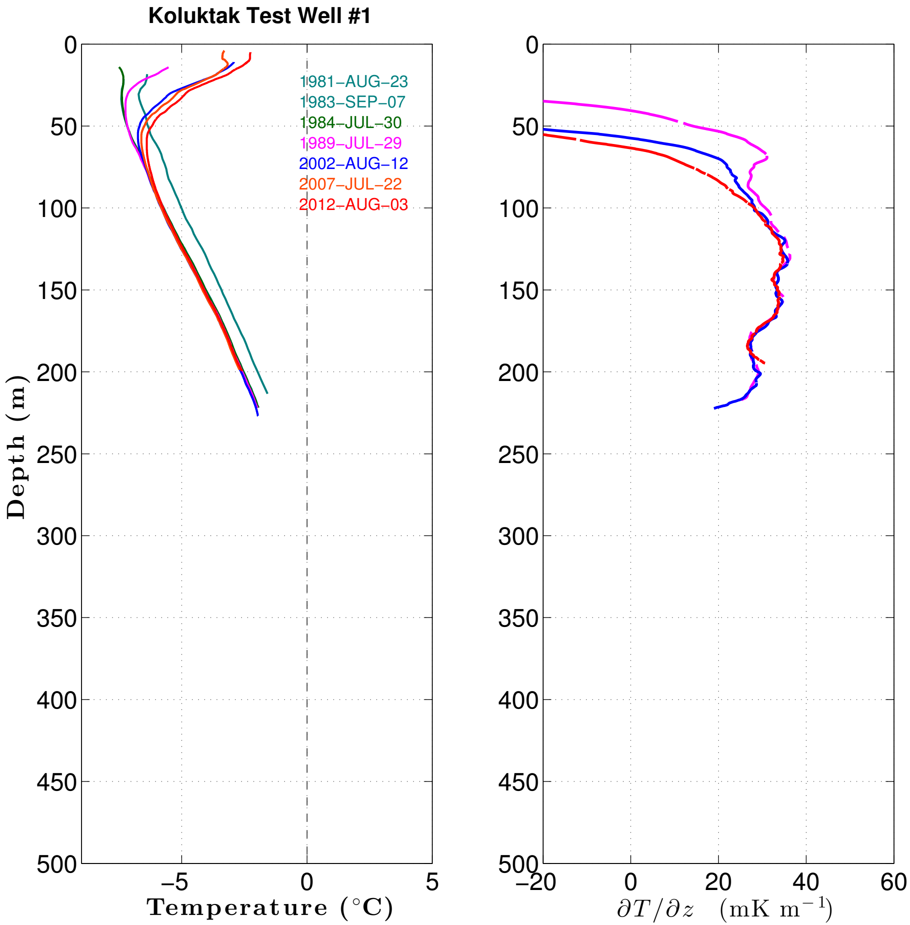

Fig. 16. Temperature profiles in the Koluktak Test Well No. 1, color-coded by acquisition date (left). Temperature gradients calculated from the 1989, 2002, and 2012 logs are shown in the right panel. The accessible portion of this well does not reach the base of permafrost.

ESSDD
7, 1–57, 2014

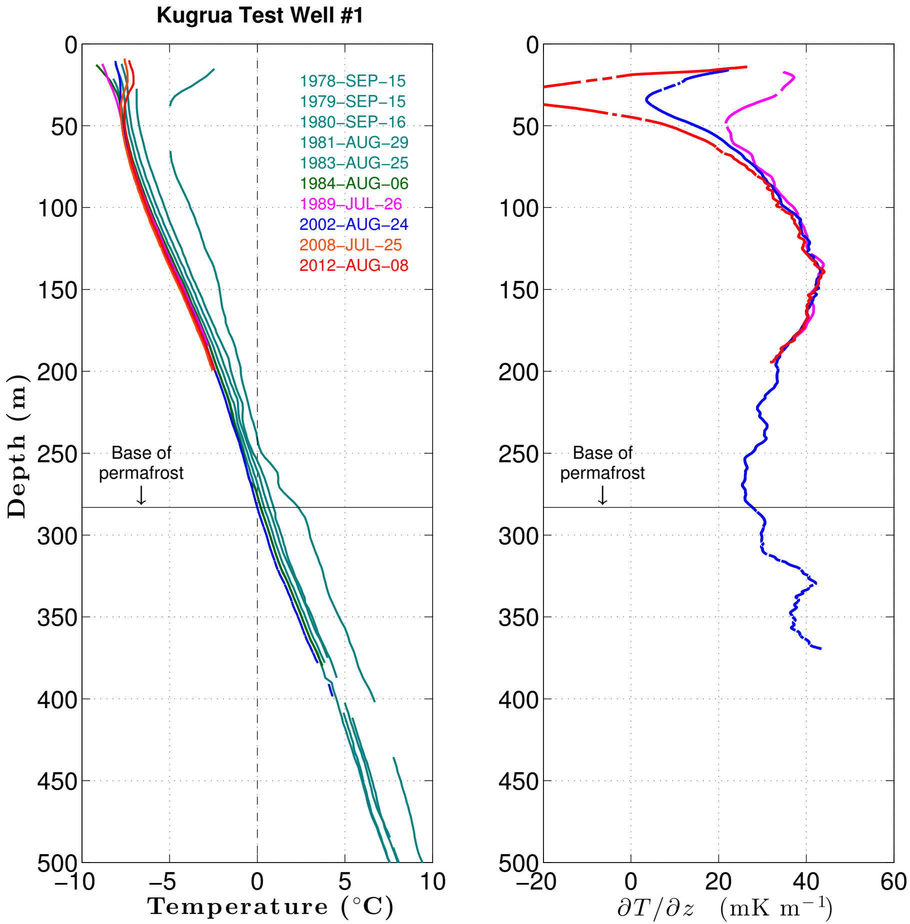

Fig. 17. Temperature profiles in the Kugrua Test Well No. 1, color-coded by acquisition date (left). Temperature gradients calculated from the 1989, 2002, and 2012 logs are shown in the right panel.

ESSDD
7, 1–57, 2014

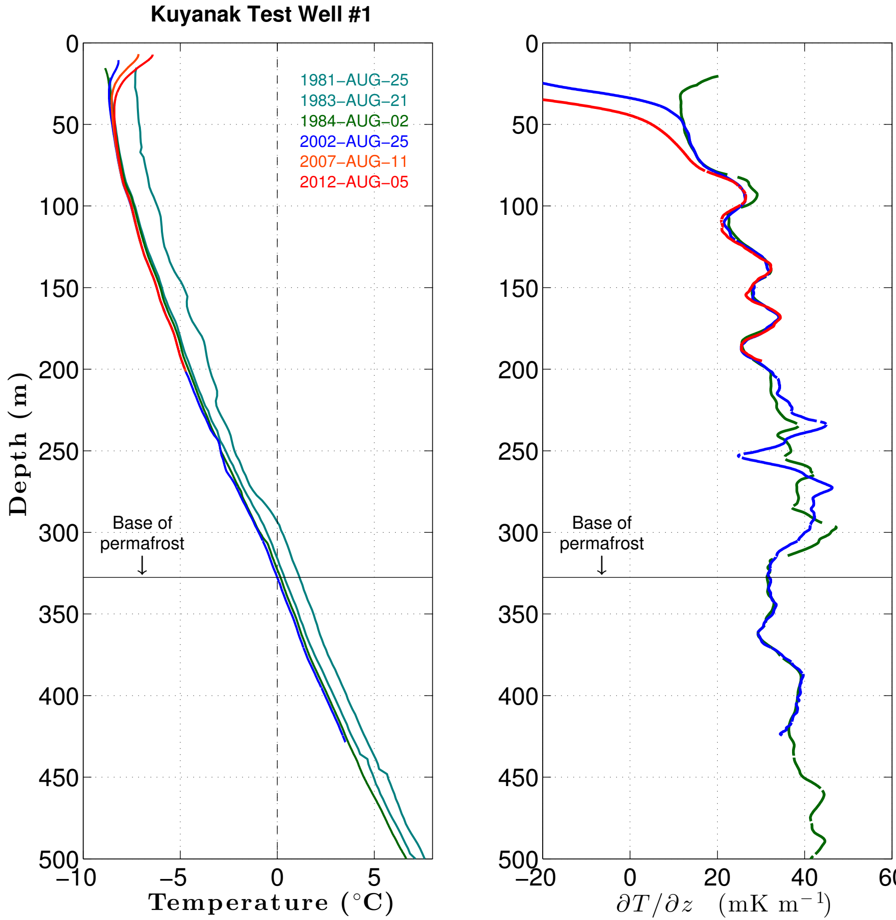

Fig. 18. Temperature profiles in the Kuyanak Test Well No. 1, color-coded by acquisition date (left). Temperature gradients calculated from the 1984, 2002, and 2012 logs are shown in the right panel.

ESSDD
7, 1–57, 2014
Temperature data from the DOI/GTN-P Deep Borehole Array
G. D. Clow

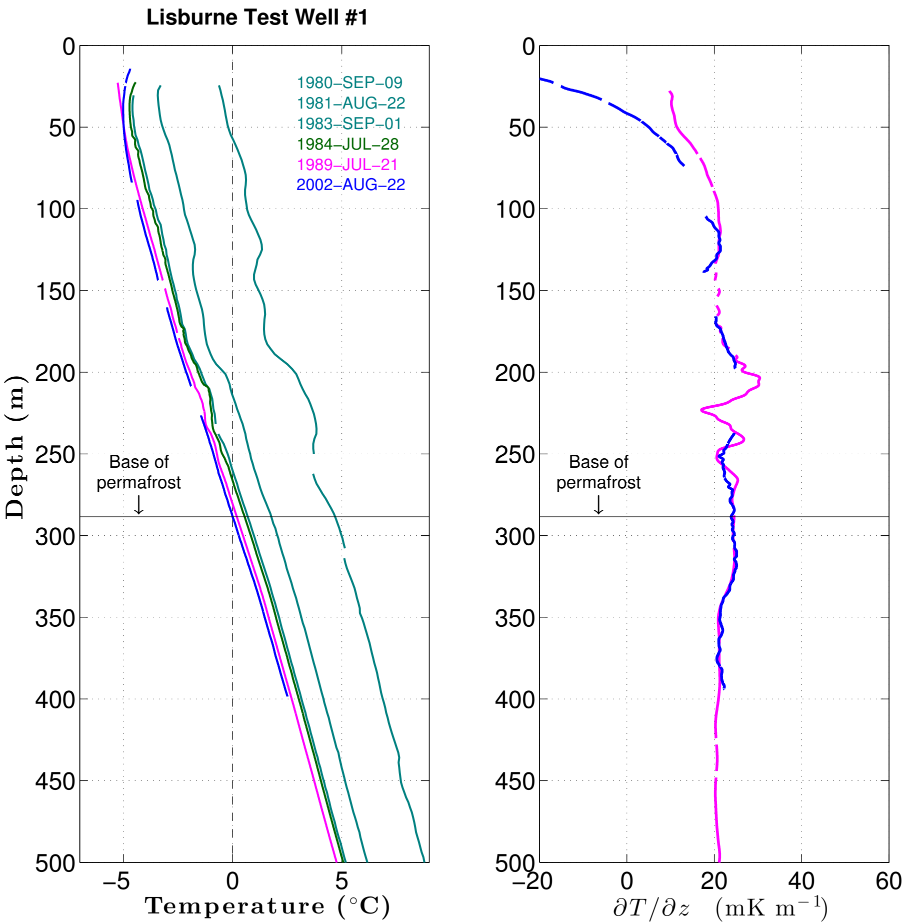

Fig. 19. Temperature profiles in the Lisburne Test Well No. 1, color-coded by acquisition date (left). Temperature gradients calculated from the 1989 and 2002 logs are shown in the right panel.

ESSDD
7, 1–57, 2014

G. D. Clow

Title Page
Abstract | Instruments
Data Provenance & Structure
Tables | Figures
◀| |▶
◀ ▶
Back | Close
Full Screen / Esc
Printer-friendly Version
Interactive Discussion

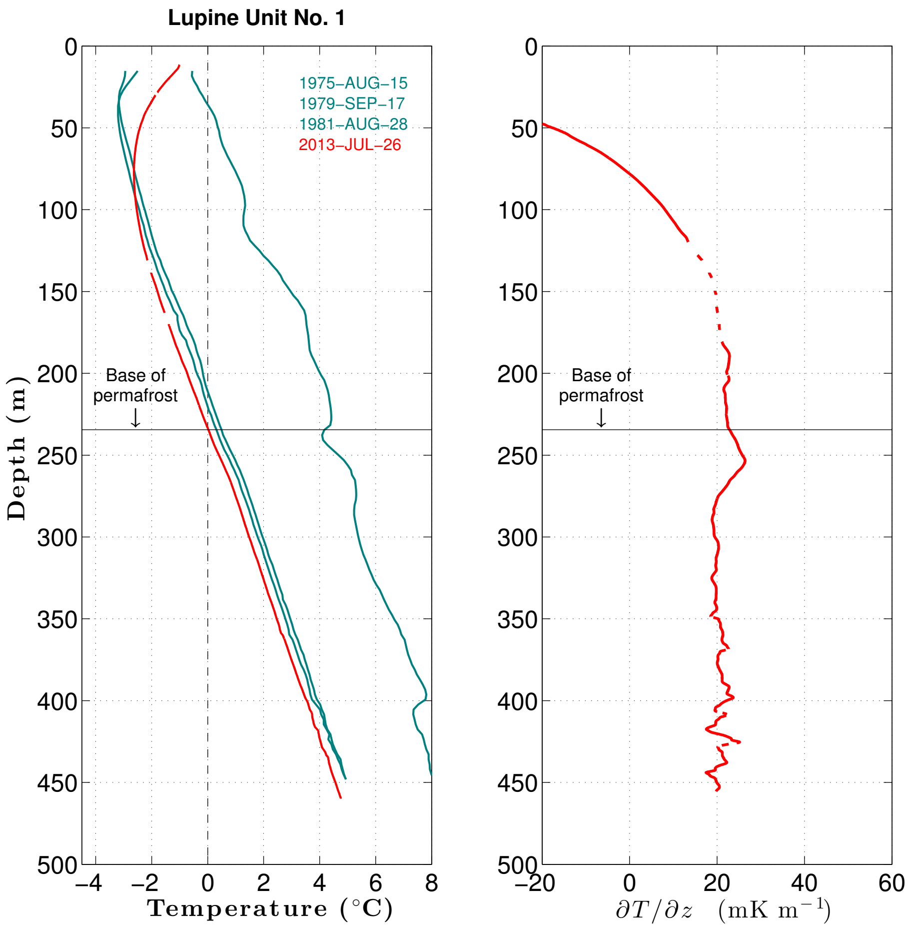

Fig. 20. Temperature profiles in the Lupine Unit No. 1 well, color-coded by acquisition date (left). The temperature gradient calculated from the 2013 log is shown in the right panel.

ESSDD
7, 1–57, 2014
Temperature data from the DOI/GTN-P Deep Borehole Array
G. D. Clow

Title Page
Abstract
Instruments
Data Provenance & Structure
Tables
Figures
◀◀
▶▶
◀
▶
Back
Close
Full Screen / Esc
Printer-friendly Version
Interactive Discussion

ESSDD
7, 1–57, 2014

Temperature data from the DOI/GTN-P Deep Borehole Array

G. D. Clow

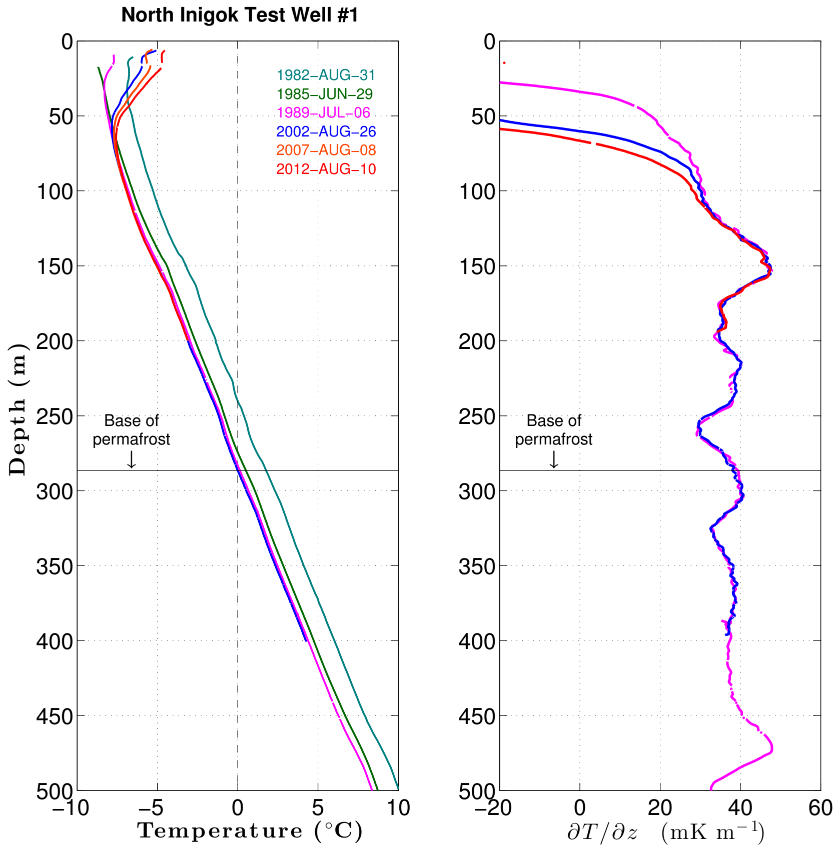

Fig. 21. Temperature profiles in the North Inigok Test Well No. 1, color-coded by acquisition date (left). Temperature gradients calculated from the 1989, 2002, and 2012 logs are shown in the right panel.

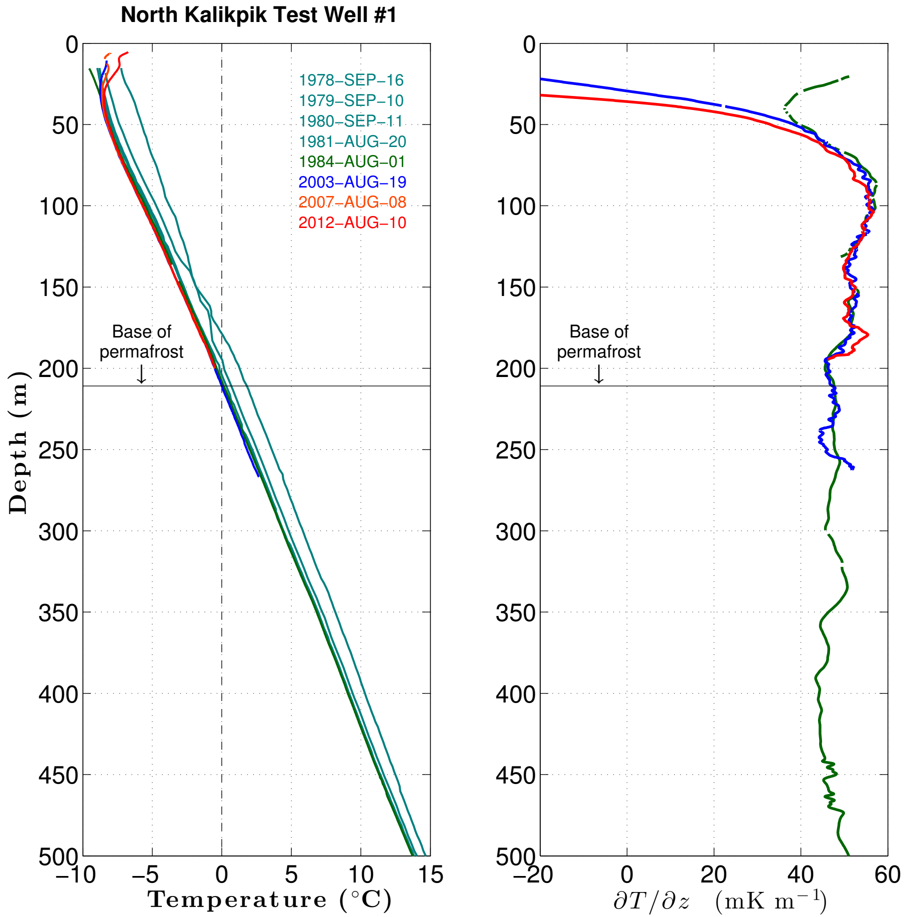

Fig. 22. Temperature profiles in the North Kalikpik Test Well No. 1, color-coded by acquisition date (left). Temperature gradients calculated from the 1984, 2003, and 2012 logs are shown in the right panel.

ESSDD
7, 1–57, 2014

Temperature data from the DOI/GTN-P Deep Borehole Array

G. D. Clow

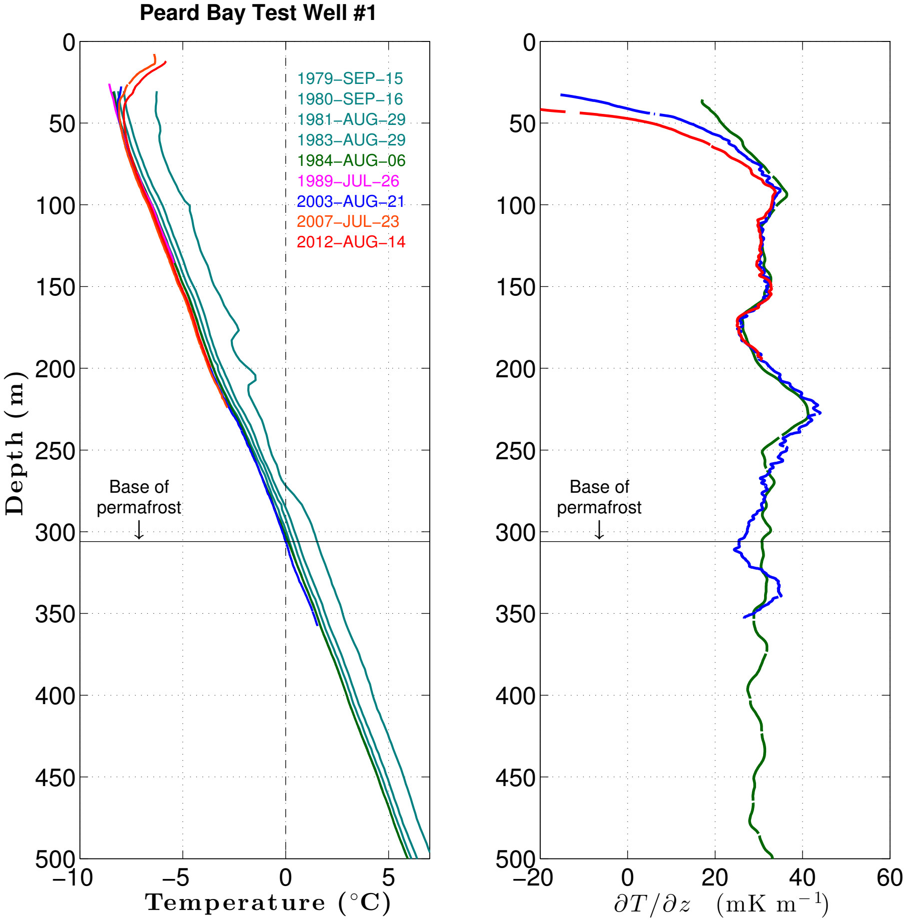

Fig. 23. Temperature profiles in the Peard Bay Test Well No. 1, color-coded by acquisition date (left). Temperature gradients calculated from the 1984, 2003, and 2012 logs are shown in the right panel.

ESSDD
7, 1–57, 2014

Temperature data from the DOI/GTN-P Deep Borehole Array

G. D. Clow

Title Page
Abstract
Instruments
Data Provenance & Structure
Tables
Figures
Back
Close
Full Screen / Esc
Printer-friendly Version
Interactive Discussion

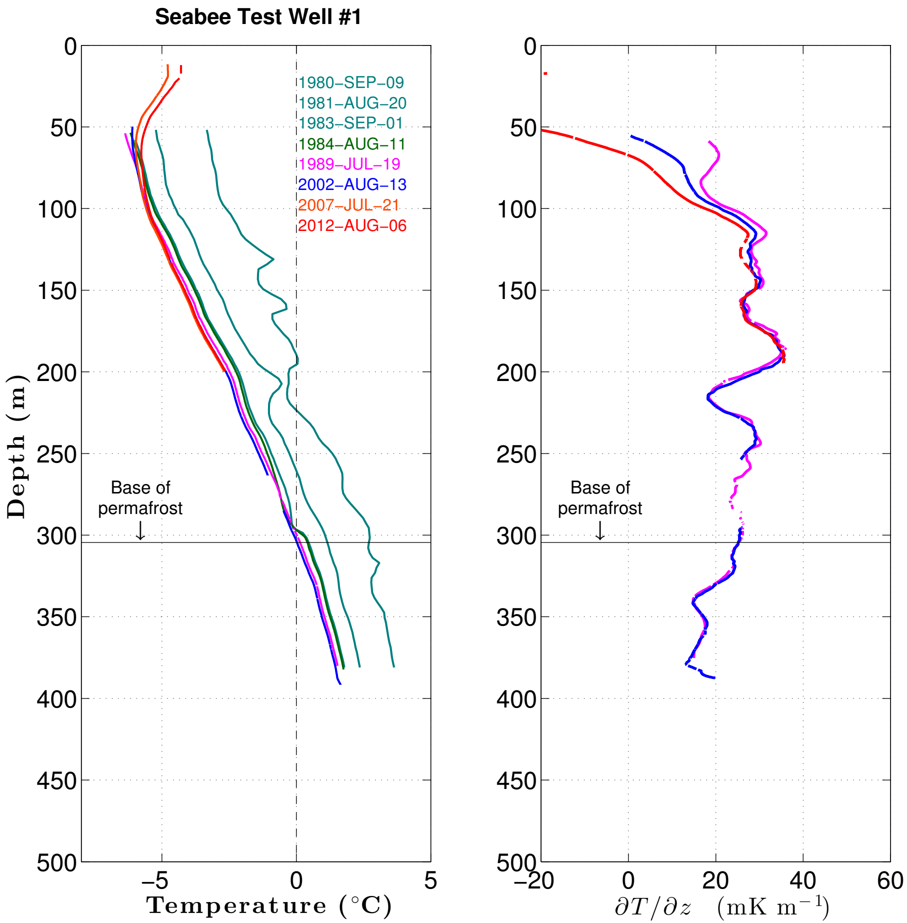

Fig. 24. Temperature profiles in the Seabee Test Well No. 1, color-coded by acquisition date (left). Temperature gradients calculated from the 1989, 2002, and 2012 logs are shown in the right panel.

ESSDD
7, 1–57, 2014

Temperature data from the DOI/GTN-P Deep Borehole Array

G. D. Clow

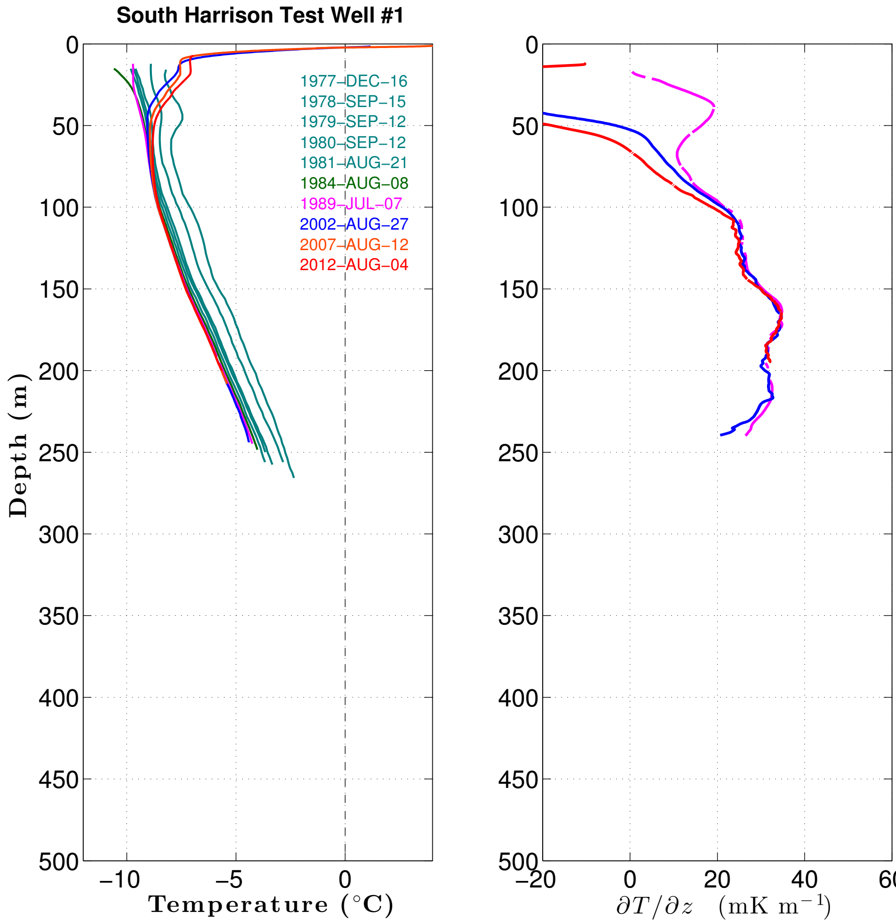

Fig. 25. Temperature profiles in the South Harrison Test Well No. 1, color-coded by acquisition date (left). Temperature gradients calculated from the 1989, 2002, and 2012 logs are shown in the right panel. The accessible portion of this well does not reach the base of permafrost.

ESSDD
7, 1–57, 2014

Temperature data from the DOI/GTN-P Deep Borehole Array

G. D. Clow

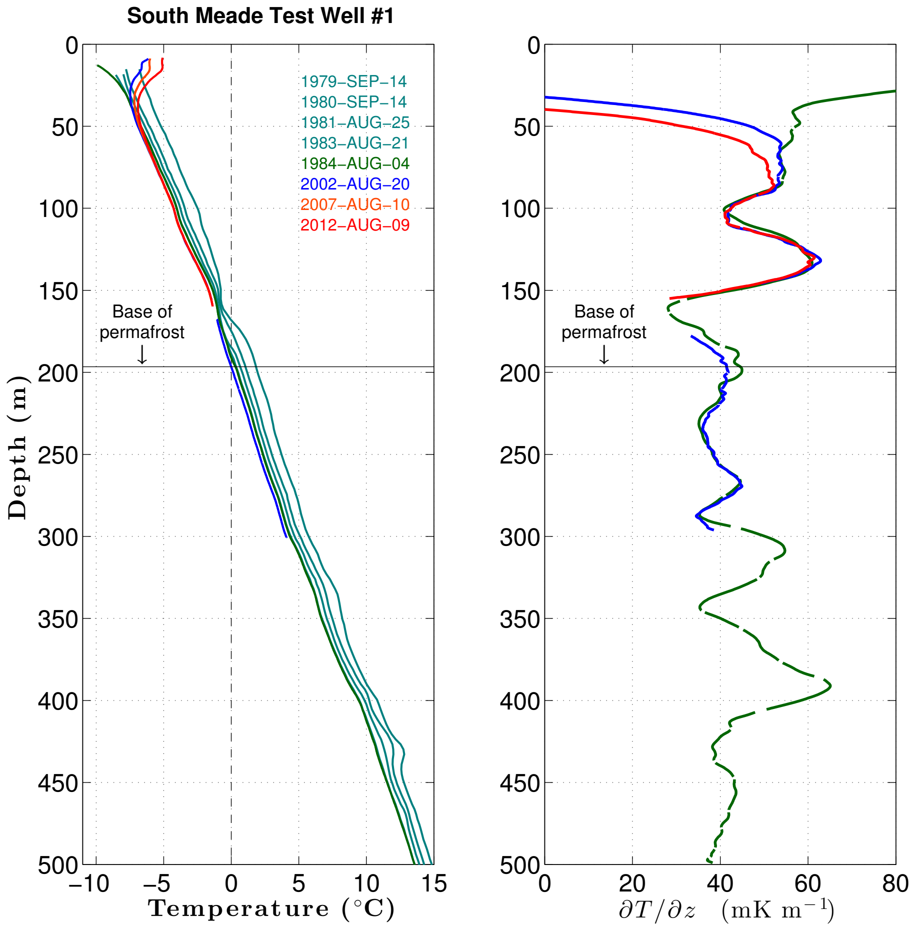

Fig. 26. Temperature profiles in the South Meade Test Well No. 1, color-coded by acquisition date (left). Temperature gradients calculated from the 1984, 2002, and 2012 logs are shown in the right panel.

ESSDD
7, 1–57, 2014

Temperature data from the DOI/GTN-P Deep Borehole Array

G. D. Clow

Title Page
Abstract
Instruments
Data Provenance & Structure
Tables
Figures
◀
▶
Back
Close
Full Screen / Esc
Printer-friendly Version
Interactive Discussion

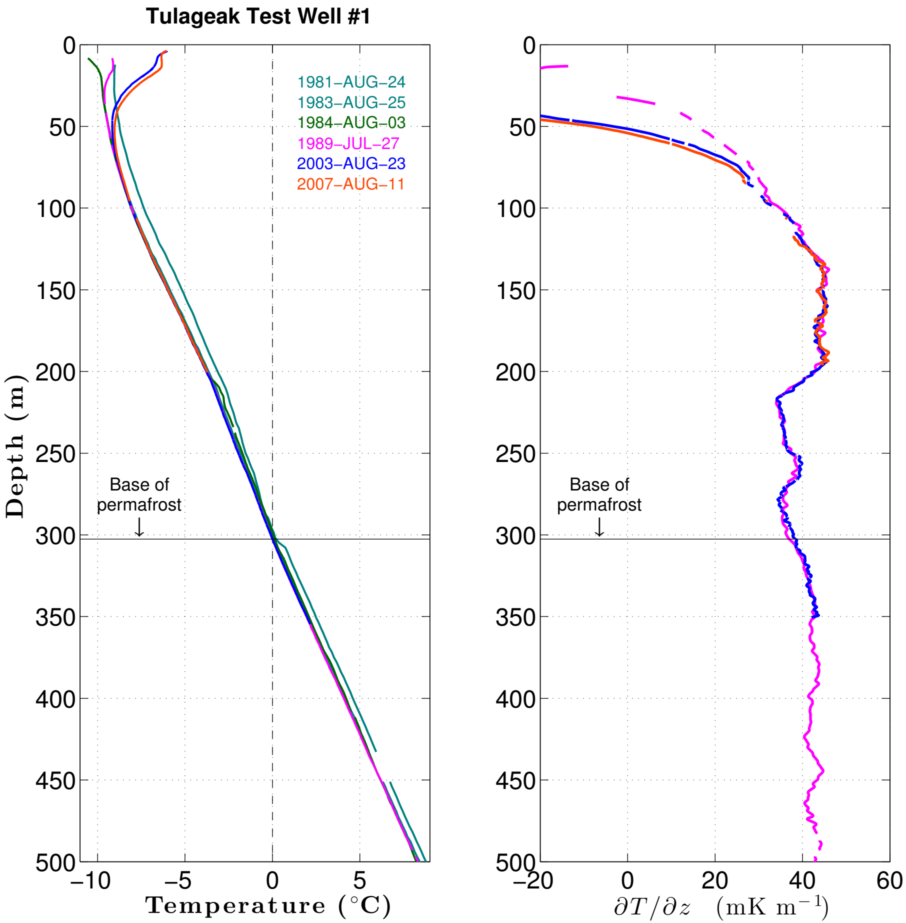

Fig. 27. Temperature profiles in the Tulageak Test Well No. 1, color-coded by acquisition date (left). Temperature gradients calculated from the 1989, 2003, and 2007 logs are shown in the right panel.

ESSDD
7, 1–57, 2014

Temperature data from the DOI/GTN-P Deep Borehole Array

G. D. Clow

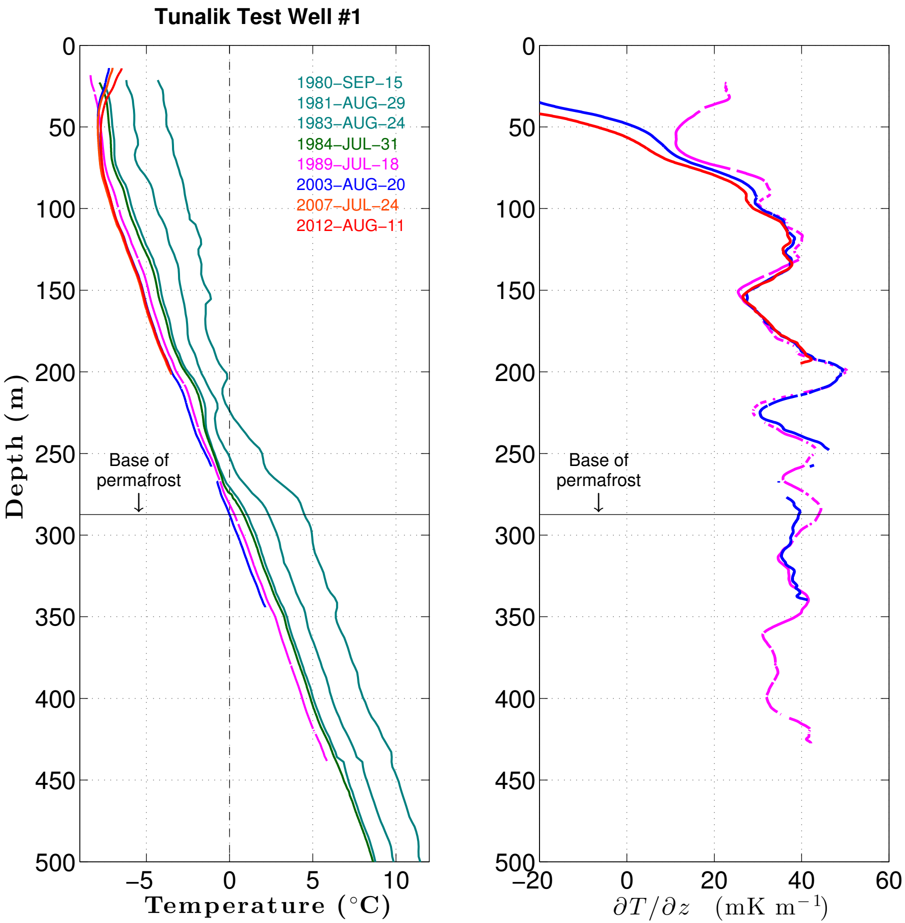

Fig. 28. Temperature profiles in the Tunalik Test Well No. 1, color-coded by acquisition date (left). Temperature gradients calculated from the 1989, 2003, and 2012 logs are shown in the right panel.

ESSDD
7, 1–57, 2014
Temperature data from the DOI/GTN-P Deep Borehole Array
G. D. Clow

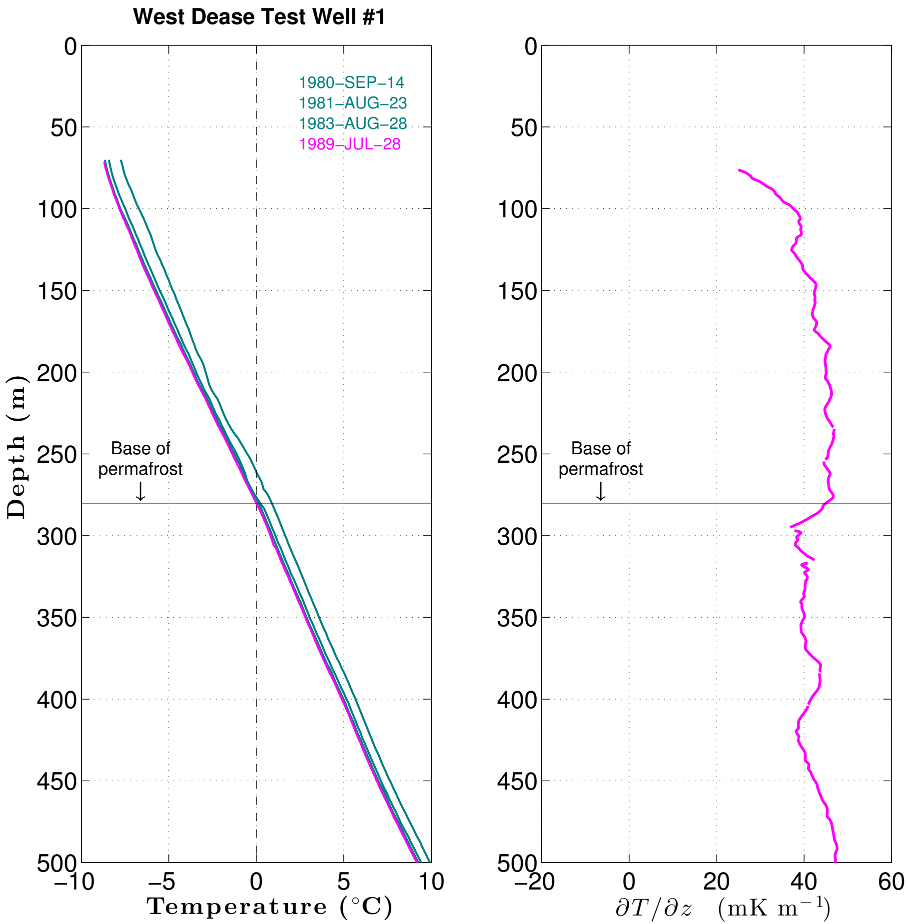

Fig. 29. Temperature profiles in the West Dease Test Well No. 1, color-coded by acquisition date (left). Temperature gradient calculated from the 1989 log is shown in the right panel.

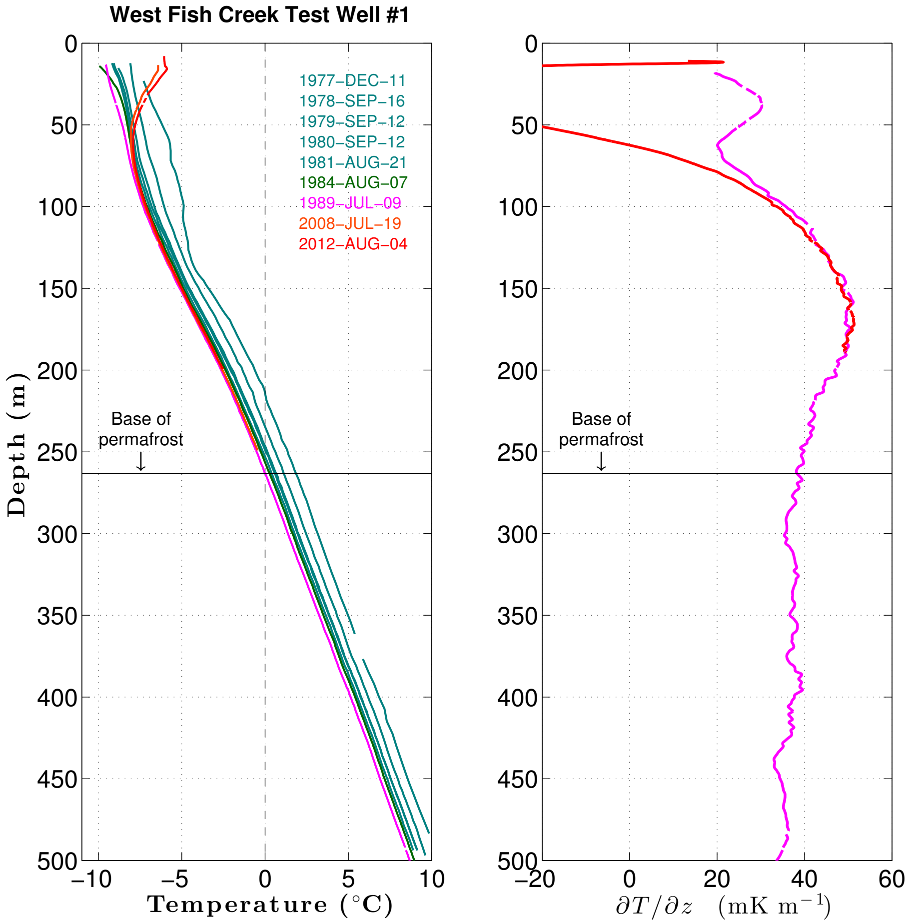

Fig. 30. Temperature profiles in the West Fish Creek Test Well No. 1, color-coded by acquisition date (left). Temperature gradients calculated from the 1989 and 2012 logs are shown in the right panel.

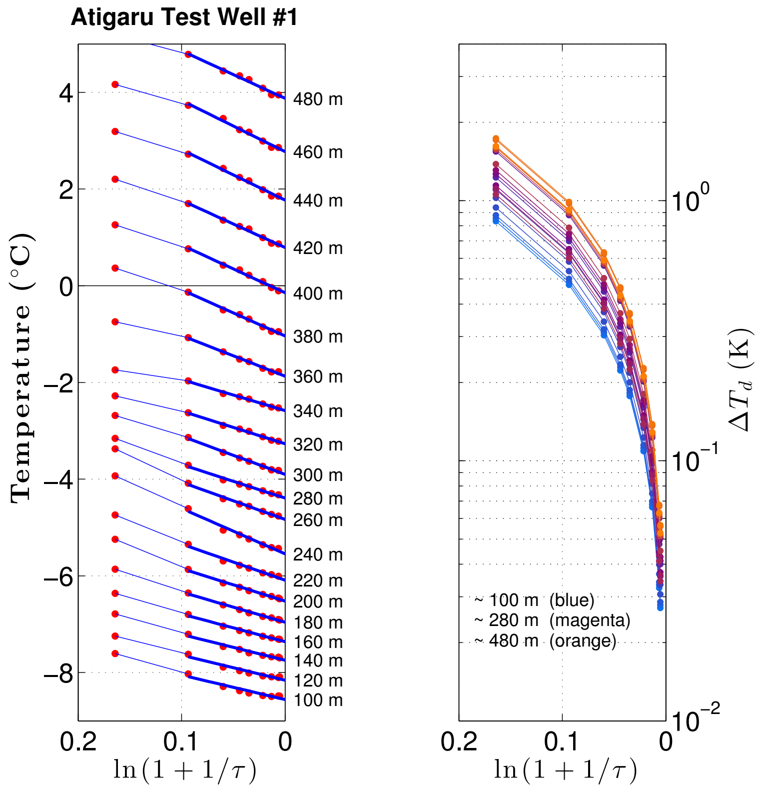

Fig. 31. Recovery of temperatures from the thermal drilling disturbance at fixed depths in the Atigaru Test Well No. 1 (left). In this case, the earliest log was obtained at dimensionless time $\tau = 5.6$, or $\ln(1 + 1/\tau) = 0.16$. Complete thermal recovery occurs as $\ln(1 + 1/\tau)$ approaches zero ($\tau \to \infty$). A least-squares fit to the temperature data for times $\tau > 8$ provides values for the undisturbed temperature profile $T_o(z)$ and the factor $\bar{q}_l/(4\pi K)$ (dark blue lines). With these values, the evolution of the thermal drilling disturbance ΔT_d (right panel) can be found using Eqs. (13) and (14).

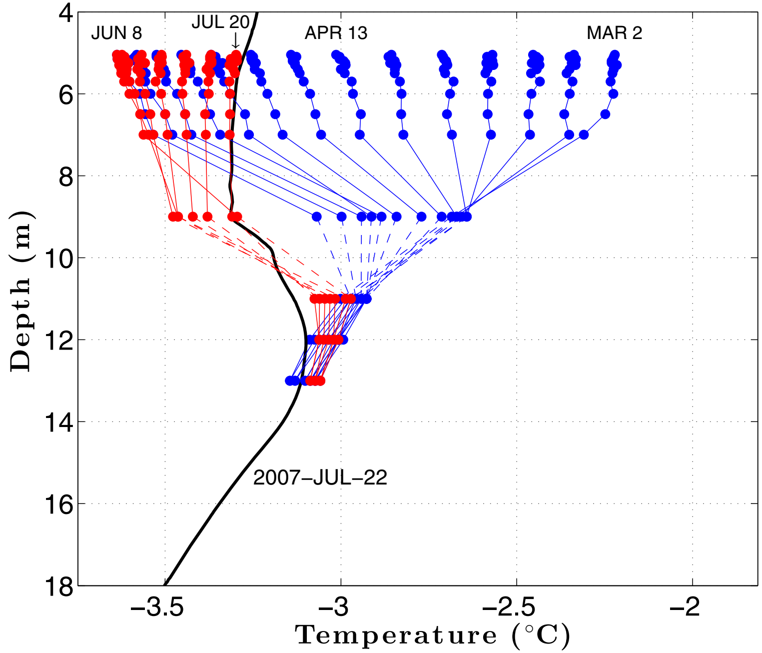

Fig. 32. Temperatures in the Koluktak Test Well No. 1 measured by a thermistor string extending over the 5–13 m depths from 2 March through 20 July (2007); thermistor string temperatures are displayed once per week. The thermistor string was removed from the well and a standard borehole temperature log acquired on 22 July 2007 (black line). The thermistor string data confirm the development of a nearly-isothermal zone in the upper 10 m of the well due to intense convection during the spring and early summer.

ESSDD
7, 1–57, 2014

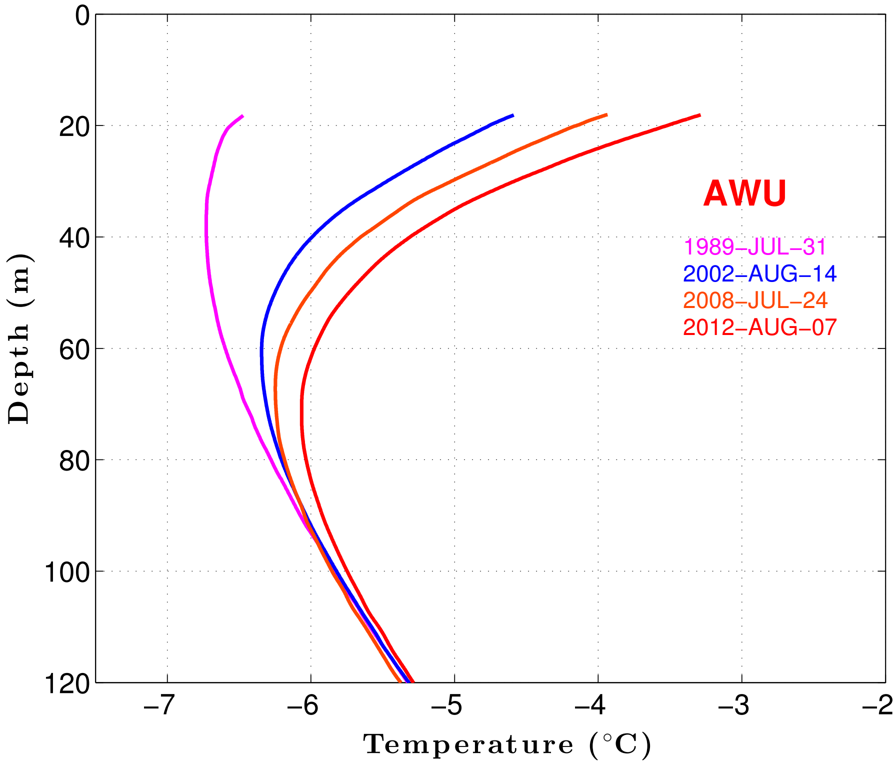

Fig. 33. Upper portion of the last four temperature logs from the Awuna Test Well No. 1. Near-surface permafrost temperatures have warmed substantially at this site since the late 1980s in response to climate change. Seasonal effects in the upper 18 m have been removed to more clearly show the climate signal.

ESSDD
7, 1–57, 2014

G. D. Clow